A TIMED COLOURED PETRI NET MODEL OF THE SAXS/WAXS MEASUREMENT PROTOCOL FOR HYDRATED ARTICULAR CARTILAGE: RESOURCE-AWARE SIMULATION, STATISTICAL ANALYSIS AND COMPARISON WITH PROTOCOL, DOSE AND DATA-ANALYSIS MODELS

Sofoklis Christoforidis

Efstathios Titopoulos

Assoc. Prof. PhD Eng. Boriana Ilieva

Assoc. Prof. PhD Eng. Georgi Stanchev

Technical University of Sofia, Sofia, Bulgaria

Eleni Kromitoglou

Prof. Nikolaos Vordos

Dimosthenis Pappas

Democritus University of Thrace, Kavala, Greece

Abstract. For the investigation of small- and wide-angle X-ray scattering (SAXS/WAXS) of hydrated articular-cartilage explants a multi-day measurement program has to be performed. The sample preparation, radiation damage, available beamtime, lab manpower and equipment all interact. Thus, the currently used measurement protocols are described in the form of text and tables. However, based on these descriptions the question whether a given, planned measurement program can be completed within the allocated beamtime with which losses, and with which statistical power, cannot be answered before the actual beamtime usage starts. In the present paper a timed Coloured Petri Net (TCPN) of the complete measurement program from the joint dissection over the sample preparation, treatment, freezing, and the subsequent steps of thawing, mounting, calibration, depth line scans, three loading scenarios (static depth mapping, stress relaxation, and cyclic loading) including the subsequent remeasurement steps, data evaluation, and quality control is presented. In this net the samples under investigation are modeled as colored tokens. The tokens carry information on the treatment of the samples, the loading scenario, the

(so far) accumulated dose, the dose beyond which damage of the sample can be expected, the time elapsed after the thawing of the sample until it can be accepted for measurement, and quality flags indicating potential problems with the samples. The lab operators, the loading device, the X-ray beam, the evaluation workstation, the biosafety hood, the incubator, and the deep freezer are modeled as re-usable resources. The control tokens modeling the calibration validity, the background scattering, the radiation-dose test, and the available beamtime are used to control the progression of the measurement program. The net has an ordinary projection of 34 places and 28 transitions with an incidence matrix of rank 20. The 14 minimal P-semiflows cover all places, i.e. they prove the properties of conservativeness and boundedness of the net. The 4 minimal T-semiflows model the recalibration and the remeasurement cycles. The execution of the net was performed in Python as a discrete-event simulation of a timed CPN in 41,900 Monte Carlo replications. For a 54-explant design (three different treatments, three different loading scenarios, six different explants per measurement cell) on a 48h synchrotron beamtime with two operators the model predicts 50.9 accepted datasets (95 % confidence interval 50.8–51.0) with a rejection rate of 5.8 %. However, the probability that all cells of a measurement design contain six or more acceptable datasets is only 3.8 %, i.e. it significantly increases to 91 % if eight instead of six explants per cell are prepared. For the same measurement design on a laboratory Cu K-alpha instrument (CuKAl) 14.2 acceptable datasets (out of 17.5 expected ones) are predicted to be obtained within 80 working hours with a loss of 19 % due to dehydration. A four-factorial ANOVA is used to analyze the influence of the four factors, i.e. the beamtime allocation, the number of lab operators, the interaction of both, the exposure time, and the thaw-batch policy on the number of accepted datasets. The results are beamtime allocation 0.95 (partial eta-squared), number of operators 0.82, interaction of both 0.76, exposure time 0.46, and, finally, the thaw-batch policy 0.19. The dose–response relations of the exposure noise rule of the SAXS Guide, the radiation-damage models, the tissue-preservation studies, and the peak-fitting statistics used in the source papers are all reproduced by the model. The empirical dose and integrity models of the sample are used to parameterize the guards of the net in a hybrid architecture. The representation of the complete measurement protocol of the SAXS/WAXS investigation of cartilage using a timed Coloured Petri Net (TCPN) is, thus, significantly more complete than the representation using the currently used measurement protocols.

Keywords: small-angle X-ray scattering; articular cartilage; collagen D-period; Coloured Petri Net; discrete-event simulation; beamtime planning; radiation damage; protocol design; formal verification.

1. Introduction

Articular cartilage consists of about 90% water, organized in a nanocomposite of type II collagen fibrils embedded in a proteoglycan-rich matrix. In cartilage, proteoglycans create high osmotic swelling pressures which are counteracted by tensile pre-strain within the fibrils in the range of 1–2% of the axial D-period length (about 65 nm). Importantly, cartilage consists of different zones (tangential surface zone, transitional zone, radial zones including deep zone and, in opposition to the soft cartilage, calcified cartilage at the bone interface), thus all type of measurements must be performed in a spatial resolved manner. Synchrotron SAXS with a very small microbeam (15–50 μm²) can measure meridional orders of the D-periods from which pre-strain, intrafibrillar order and distribution width can be derived. Azimuthal intensity distribution of SAXS patterns gives information about the orientation of the corresponding fibrils within the measurement volume. WAXS, which is not used systematically so far in cartilage studies (in contrast to, e.g., bone), measures the packing of collagen molecules laterally and the degree of crystallization of the mineral phase (Giannini et al.,2014); all WAXS parameters are general knowledge (protocol), thus have not been determined in the framework of the source studies.

The two primary documents for the study at hand, synthesizing nine publications on nanocomposite biomaterials by means of Small-angle X-ray Scattering, with focus on biology and pharmacology, synthesize nine publications on nanocomposite biomaterials by means of Small-angle X-ray Scattering (SAXS) to establish a single protocol for the study of fully hydrated cartilage explants (Pabisch et al., 2013). The algorithm, based on previous studies (Inamdar et al., 2017; 2019; 2021; Moger et al., 2007) of full-thickness cartilage explants (diameter: 2 mm) punched from the metacarpophalangeal joints of adult bovines and subsequently allowed to rest in culture medium over a 24 h time frame (optional: prior treatment with chondroitinase ABC, collagenase or interleukin-1-beta) prior to freezing in PBS at -20°C or -80°C without chemical fixation, allows for a single freeze-thaw cycle of the tissue prior to measurement in micro-compression in PBS at the nanoscale (Muehleman et al., 2004). The SAXS measurements are performed with a beam-size smaller than the zone thickness of the cartilage, at a sample-to-detector distance of 0.8 to 1 m, and with exposure times between 0.03 s and 0.5 s per point. The resulting 2D intensity distributions are azimuthally and radially integrated around the 5th meridional order. The documents specifically address the key reasons for all the choices made in establishing the above-mentioned protocol, including the various fixatives that alter D-period and fibril diameter (Kelly et al., 2021), and address reasons for the choice of two different freezing temperatures, between which there is no effect on the

mechanical properties, whereas liquid nitrogen increases hysteresis (Szarko et al., 2010). The document also addresses reasons for a single freeze-thaw cycle of the fully hydrated tissue (slightly reducing the dynamic moduli) and the addition of various protease inhibitors to prevent proteoglycan release (Qu et al., 2014). Finally, the document addresses the reasons for testing for radiation damage prior to commencing a series of SAXS/WAXS measurements on hydrated cartilage, and that higher doses of radiation than used here have been shown to alter collagen (Barth et al., 2010; 2011). The second primary document for the study at hand is an adaptation of the above-mentioned algorithm to a fully equipped laboratory SAXS/WAXS instrument, with a Cu K-alpha microfocus X-ray source, and a hybrid photon-counting detector, at which the beam is of millimeter size, resulting in very long exposure times at the nanoscale (up to 3600 s per point) and at which the fully hydrated tissue samples must be sealed in a cell, since the flight path is under-evacuated (Rinnerthaler et al., 1999; Zizak, 2003).

The two source documents synthesized in this study are primarily prescriptive, thus detailing stepwise procedures (with specified time frames where applicable) that need to be completed in order to reach the study's objectives. In essence, the documents are not executable given current resources and methodologies. Allocation of beamtime is a highly sought after, scarce resource that can range from 24 hours to 72 hours or more. Hydrated cartilage post-thaw samples also have a finite lifespan. Samples can also be damaged by high doses of radiation, and the space at a beamline is generally limited to a few individuals. In addition, there is only one loading rig and one microfocus beam at our disposal, which can be used for three different loading scenarios. The main aim of this study was therefore to investigate whether a given design (e.g., three different treatments times three loading scenarios times 6 samples) can be completed in the allotted time. Other objectives were to determine the amount of potential data loss due to different failure modes, and the statistical power of the resulting data sets. None of the existing models could address these issues, as they either modeled the D-period in response to certain mechanical parameters (mechanobiological models), predicted the onset of radiation damage as a function of dose (dose models), described optimal storage conditions for preservation of cartilage samples (preservation studies), or described the analysis of D-periods from SAXS data (data-analysis models). The same lack of modeling of the process of care (i.e., the clinical pathway) exists for the study of disease progression in chronic kidney patients (Christoforidis et al., 2026).

Timed Coloured Petri Nets (TCPNs) (Jensen & Kristensen, 2009) are also appropriate for modeling the dynamics of a study within a scarce set of resources, such as a synchrotron

facility or even a laboratory, since tokens carry attributes of samples under investigation (e.g., depth, location, angle), transitions are guarded by the rules of the protocol that govern the progress of a sample through different states (activities), resources are consumed and then returned by transitions, and time-stamps are attached to tokens to record the duration of an activity. The usual structural analysis of a Place/Transition net (P- and T-invariants) (Murata, 1989) as well as the execution of the resulting net to simulate the progress of the samples, either deterministically or by Monte Carlo methods, as in a discrete-event simulation (Law, 2015), or as in a Generalized Stochastic Petri Net (Marsan et al., 1995), can be performed on such a representation. Such Nets are typically used to model and analyze business processes (van der Aalst, 1998) but have recently been used by this author to model a pre-dialysis care pathway in patients with chronic kidney disease (Christoforidis et al., 2026).

The main objectives of this study will be to (1) represent the full cartilage SAXS/WAXS protocol in form of a TCPN comprising of sample-, resource- and control-subnets, (2) to check the representation for structural correctness by means of P- and T-invariants, (3) to execute the formal model as a discrete event simulation model in Monte-Carlo fashion in order to mimic synchrotron and laboratory experiments, (4) to analyze the generated event data in more detail by means of descriptive statistics, factorial ANOVA, one-at-a-time-sensitivity-analysis, a dose-exposure-relationship, distribution fitting of times between events, a design and power analysis, an explant-level-logistic-regression and check for convergence, (5) to compare the formal representation with the models used in the source bibliography for the same protocol, and (6) to state the limitations of this approach.

2. Methodology

2.1 Study design and protocol abstraction

In a formal process-modelling study, a conceptual and analytical model was developed for the protocol described in two source documents that in total referred to 9 other publications that were synthesized by the authors of the two documents. The loading-scenarios, exposure-durations, step-sizes, translation-windows and quality-control-rules for the workflow steps were taken from the Inamdar et al. papers (2017, 2019, 2021), the depth-mapping and background-modeling rules from Moger et al. (2007), the preservation-rules for the microtissue preparations from Szarko et al. (2010), Qu et al. (2014), and Kelly et al. (2021), and the

laboratory setup from the second source document and from the SAXS Guide by Schnablegger & Singh (2011).

For a given experimental design (i.e., number of samples, number of experiments per sample) required to meet the scientific need of the experiment, the model can assess the operational feasibility of implementing that design using the available resources within the available time and identify the failure modes that will predominate under a given set of circumstances. The experimental design consisted of three groups (i.e., control, ChABC-treated, IL-1β-treated) x 3 scenarios (i.e., depth-mapping alone, depth-mapping + stress-relaxation, cyclic loading) x 6 explants (i.e., 54 total explants) obtained from 7-9 joints. A model time unit is one minute. This model represents time from joint receipt on day 0 to completion of processing 72 hours following the end of the scheduled beamtime on day 28 (12 days for IL-1β treatment + 24 hours for tissue to return to room temperature + 2 weeks for storage at frozen state + day of beamtime).

2.2 Coloured Petri Net specification

The net is defined as the CPN = (P, T, A, Sigma, V, C, G, E, I), where P is the set of places, T the set of transitions, A the set of arcs, Sigma the set of color sets, V the set of variables, C the color function assigning a color set to each place, G the guard function, E the arc function expressing the arc properties, and I the initialization function. The three-color sets used are the SAMPLE record (id, joint, group, scenario, thaws, t_thaw, t_mount, t_measured, integrity_time, damage_threshold, dose_max, frames, remeasures, exposure_factor, flags, verdict, reason, history), the UNIT color set of indistinguishable resource tokens, and the CTRL color set of control tokens. A token of the CTRL color set is a calibration token, which carries the time of the last calibration. The timed semantics of this net are described in detail in CPN Tools (Jensen et al., 2007). Briefly, every token has a time stamp. A transition i is enabled at model time t if there exists a binding b of the input places of i such that for all k in the binding, the time stamp of the token k at t_k <= t, and G_i(b) = true. A transition fires instantly, and for each output place of i in the binding, a token with the same color as the token in the input place of i in the binding, and the time stamp t + delta_i, is created and placed in the output place. A busy resource is modeled as a resource token that is put back to the corresponding place with a future time stamp. When no transition is enabled in the net, the model time is advanced to the earliest time stamp found in the net. Figure 1 shows the net.

Figure 1. Timed Coloured Petri Net of the cartilage SAXS/WAXS protocol (34 places, 28 transitions)

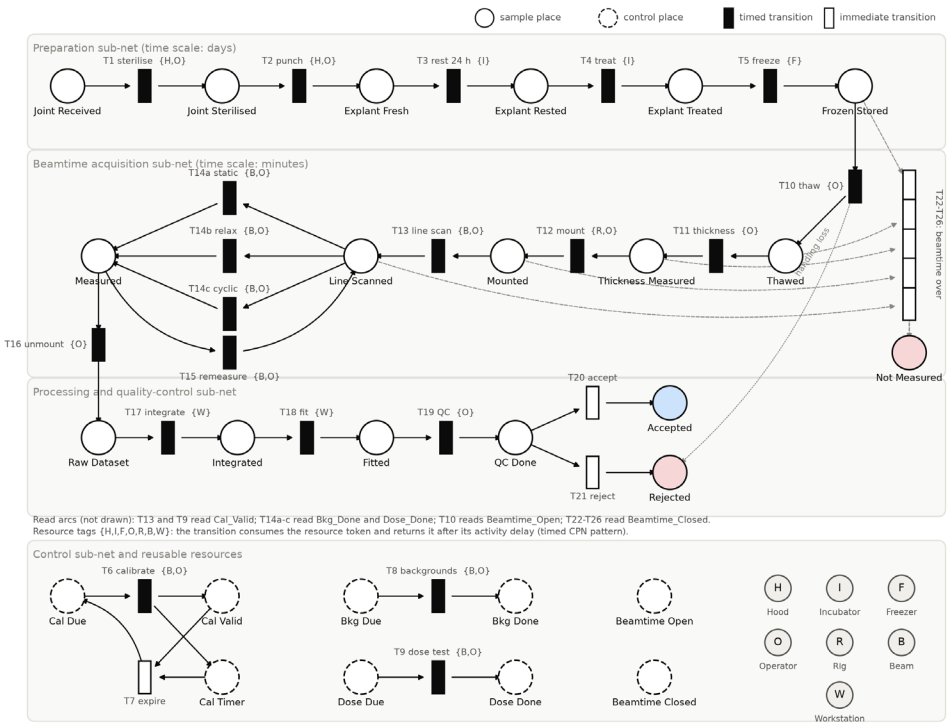


Figure 1. Timed Coloured Petri Net of the cartilage SAXS/WAXS protocol. Sample places are drawn as solid circles, control places as dashed circles and resource places as grey discs; filled bars are timed transitions and open bars immediate transitions. Resource tags in braces list the resource tokens consumed and returned by each transition. Read arcs and the dashed end-of-beamtime arcs are described in the figure text.

2.3 Sample, resource, control and temporal sub-nets

The ordinary projection contains 18 sample-state places, 7 resource places and 9 control places, a total of 34 places, and 28 transitions (20 timed and 8 immediate). The places and transitions of the ordinary projection are listed in Table 1 and Table 2, respectively. The 7 resource places are assigned to biosafety hood, incubator slots, freezer slots, operators, micro-compression rig, beam (or laboratory instrument) and the processing workstation. As noted for the activities, a transition that requires a resource will only fire if there is an explant token and a resource token in the place simultaneously, and this reusable resource token is then returned after the activity delay has expired. The control sub-net is used to model three validity functions: the calibration (for the silver behenate and collagen standard) that is only valid for 12 hours and must then be renewed before the beam can be used again for sample measurement, the

backgrounds recording that is only done once per beamtime, and the radiation-dose test. Furthermore, the beamtime window can be opened and closed using this control sub-net.

The durations for manual steps (sterilizing, punching samples, thawing samples, thickness measurements, mounting samples, unmounting samples, calibration, backgrounds, quality control, combining images, fitting) are lognormally distributed around the given scenario parameter values with a coefficient of variation of 0.2. For the beamline set-up steps (e.g. rest, treatment, line scan, loading scenarios) the durations are deterministic but include a uniform random variable of up to 5 % to model overhead. The line scan in Static depth mapping goes to a depth of 2 mm in 20-micron steps so that 100 points in total are measured, each with the duration of the exposure plus a constant overhead for moving to the next point and reading out the data. So, a scenario parameter for the scan duration of 0.5 s results in a total duration of 2.5 min for the scan. The compression in Static depth mapping is modeled as a simple ramp to 20 % strain at 20 % per minute. After that the sample is relaxed for 15 min and then a second line scan is performed. In Stress relaxation the sample is held at 20 % strain for 900 s with 15 frames of 10 s each followed by frames of 60 s each. In Cyclic loading the sample is cyclically loaded between 0 % and 20 % strain 150 times at a frequency of 0.25 Hz. There are 1 s pauses between the cycles. Frames are acquired every 5th cycle.

Table 1. Places of the net grouped by sub-net (34 places).

Place(s)	**Sub-net**	**Meaning / initial marking**
Joint_Received, Joint_Sterilised	sample	joint tokens before and after surface sterilization (detergent, 70 % ethanol)
Explant_Fresh, Explant_Rested, Explant_Treated	sample	2 mm full-thickness explants after punching, after 24 h rest at 37 C, after treatment
Frozen_Stored	sample	explants in PBS at -20 / -80 C; freezer slot held until thaw
Thawed, Thickness_Measured	sample	single thaw and PBS equilibration; thickness with calibrated calliper
Mounted, Line_Scanned, Measured	sample	on the loading rig: preloaded 0.1 N; depth line scan done; loading scenario done (rig held)
Raw_Dataset, Integrated, Fitted, QC_Done	sample	patterns with synchronised mechanical data; I(q) and I(chi); D, IFO, w_q, chi_0, w_chi fitted; QC verdict
Accepted, Rejected, Not_Measured	sample	terminal outcomes (rejection reason in the colour)
Hood, Incubator, Freezer	resource	1 biosafety hood; 60 incubator slots; 100 freezer slots
Operator, Rig, Beam, Workstation	resource	2 operators (1 in the laboratory); 1 micro-compression rig; 1 beam / instrument; 1 workstation
Cal_Due, Cal_Valid, Cal_Timer	control	calibration state and 12 h validity timer
Bkg_Due, Bkg_Done, Dose_Due, Dose_Done	control	backgrounds (empty cell with PBS, dark current) and exposure-series dose test, once per beamtime
Beamtime_Open, Beamtime_Closed	control	timed tokens that open and close the beamtime window

Table 2. Transitions of the net with resources, control tokens and nominal timing (synchrotron baseline).

Id	Transition	Resources	Control tokens read / consumed	Nominal timing
T01	Sterilize joint	Hood, Operator		15 min
T02	Punch 2 mm explants	Hood, Operator		20 min; 6-10 explants per joint
T03	Rest 24 h, 37 C	Incubator		1440 min
T04	Treatment (CTRL/ChABC/IL-1b)	Incubator		0 / 1440 / 17280 min (CTRL / ChABC / IL-1b)
T05	Flash-freeze, store -80 C	Freezer		5 min flash freeze; storage until thaw
T06	Calibrate (AgBe, collagen std)	Beam, Operator	Cal_Due	20 min; valid 720 min
T07	Calibration expires		Cal_Timer, Cal_Valid	immediate
T08	Record backgrounds	Beam, Operator	Bkg_Due	10 min
T09	Radiation-dose test	Beam, Operator	Dose_Due, Cal_Valid	10 min
T10	Thaw and equilibrate in PBS	Operator	Beamtime_Open	30 min; pipeline limit 4; cut-off 90 min before end
T11	Thickness (+/-10 um)	Operator		5 min
T12	Mount in rig, preload 0.1 N	Rig, Operator		10 min
T13	Initial depth line scan (zones)	Beam, Operator	Cal_Valid	100 x (0.5 + 1.0) s = 2.5 min
T14a	Static depth mapping (0 -> 20 % strain)	Beam, Operator	Bkg_Done, Dose_Done	1 + 15 + 2.5 min
T14b	Stress relaxation (20 %, 900 s)	Beam, Operator	Bkg_Done, Dose_Done	1 + 15 min, 27 frames
T14c	Cyclic loading (150 cycles, 0.25 Hz)	Beam, Operator	Bkg_Done, Dose_Done	15 + 1 min, 30 frames
T15	Remeasure at new position	Beam, Operator		3 min; once; halves exposure after radiation flag
T16	Unmount, release rig	Operator		5 min
T17	Azimuthal/radial integration I(q), I(chi)	Workstation		10 min
T18	Fit D, IFO, w_q, chi0, w_chi	Workstation		15 min
T19	QC: dose, hydration, fit, sync	Operator		10 min
T20	Accept dataset			immediate
T21	Reject dataset			immediate
T22	Beamtime over: still frozen		Beamtime_Closed	immediate at end of beamtime
T23	Beamtime over: thawed, unmeasured		Beamtime_Closed	immediate
T24	Beamtime over: unmeasured		Beamtime_Closed	immediate
T25	Beamtime over: mounted, unmeasured		Beamtime_Closed	immediate
T26	Beamtime over: scanned only		Beamtime_Closed	immediate

2.4 Guards, dose and integrity sub-models and outcomes

The guards, for the Thaw and Thawed protocols, check for the single-thaw rule. Thawing is allowed only during the beamtime, for explants that have not been thawed yet, with less than four other explants in the handling pipeline, and with at least 90 minutes of beamtime left. The line scan and loading scenarios, for which also a valid calibration token and a start time that allows the activity to end before the end of the beamtime has to be given, select an explant based on the scenario color of the token, read the background and dose-test tokens and

proceed as described for the scenarios. After the beamtime five immediate transitions move all explants that have not been measured yet to the Not_Measured outcome. The handling loss with probability 0.02 at thawing of an explant makes it disappear from the model before it can be measured.

To generate token colors for the dose and integrity of the explants, two sub-models were defined. The dose sub-model accumulates the largest dose for each explant at all positions. This results in line scan exposing each point once, static mapping exposing the same points twice, stress relaxation exposing 27 frames of 500s (total 27*500s) distributed over the 25 fresh positions of the 500µm translation window at 20µm pitch (two positions are exposed twice). Cyclic loading exposure of 30*0.03s (0.9s) is distributed over the 25 positions. The damage threshold for each explant is drawn from a lognormal distribution with a median of 5s and log-standard deviation of 0.4. The relative source brightness of 20 represents the ESRF ID02 configuration where 0.03s exposures were chosen (Inamdar et al., 2021). The integrity sub-model draws the time to loss of integrity for each explant from a Weibull distribution with shape parameter 3 and scale parameter 10h (measured from the moment of thawing, Qu et al., 2014) at the synchrotron or 6h (measured from the moment of mounting in the sealed Kapton cell in the laboratory, dehydration under vacuum, Inamdar et al., 2019).

The live check of quality on each final scenario transitions the first frame vs. the last frame. If a scenario has caused radiation damage to the explant, the token is marked with a radiation flag. With probability 0.05 a “problem” with parasitic scattering or fitting is randomly detected. The flagged explant is remeasured at a new position with dose reduced by half, if there is enough time left during beamtime, according to the protocol. The quality-control transition after unmounting, integration and fitting decides between rejection of radiation damage, loss of integrity, fit failure, or even a mechanical synchronization failure with probability 0.02, and acceptance. A handling loss with probability 0.02 at the moment of thawing of an explant makes it disappear from the world before it is ever measured.

2.5 Structural verification

To support conventional Petri-net analysis of the model the coloured net was mapped onto its corresponding Place/Transition net with 34 places and 28 transitions (see Figure 2). For this purpose input- and output-incidence matrices Pre and Post of dimension 34x28 were computed. The rank of the structural incidence matrix C=Post-Pre equals 20. Consequently, the

dimension of the right kernel of C^t (the P-invariant space) is equal to 14, whereas the dimension of the left kernel (the T-invariant space) is 8. Minimal non-negative semiflows have been computed by means of a Farkas / Fourier-Motzkin algorithm (Martinez & Silva, 1982; Colom & Silva, 1991). The set of 14 minimal P-semiflows is presented in Table 3. Sample conservation is expressed by one single P-semiflow covering all 18 sample places, i.e. the rig, by one single P-semiflow (Rig + Mounted + Line_Scanned + Measured = 1), which proves that in the loading rig area at most one explant can be present, the freezer area by one single P-semiflow (Freezer + Frozen_Stored = 100), five single-resource P-semiflows for hood, incubator, operators, beam, and workstation, and four P-semiflows for the four control places, i.e. Cal_Due + Cal_Valid = 1, Cal_Due + Cal_Timer = 1, Bkg_Due + Bkg_Done = 1, and Dose_Due + Dose_Done = 1. The two beamtime-window invariants were included in order to specify the time frame for the beamtime sessions. All places are covered by the P-semiflows computed from the P-invariant space, which means that the net is conservative and, according to the semiflows and the initial marking, even structurally bounded. In particular, the rig-dependent places are 1-bounded, whereas the control places are all safe. The set of 4 minimal T-semiflows consists of the cycle of the calibration and the expiration of the calibration (Calibrate, Expire_Calibration), and the three remeasurement cycles, i.e. scenario and Remeasure_New_Position for each of the three different setup-scenarios. Note that the acyclic sample pipeline in the workflow-model under study is not covered by any T-semiflow, since in such workflow-models every explant token is terminated in an outcome place (van der Aalst, 1998). All runs terminated without any deadlocks and all replications ended in a marked terminal state, where all explants had reached their respective outcome places.

Several clinically important updates affect a token’s color but not its location, i.e., dose accumulation, halved exposure due to radiation flag, updating a parasitic flag to be “raised” or “cleared” and the single “thaw” counter. Also, the fan-out of a single joint to 6 to 10 explants is a color-level feature, i.e., in the projected gray net all arcs have unit weight. Hence, in the projected net the sample places are still constrained by the structural bound of 10 for “sample units”, whereas the designed net has a bound of 54 for the “joint” sample units. If properties depending on these attributes were to be verified by state-space analysis, color-refined state spaces would have to be generated instead; all properties of interest, however, were verified using simulation.

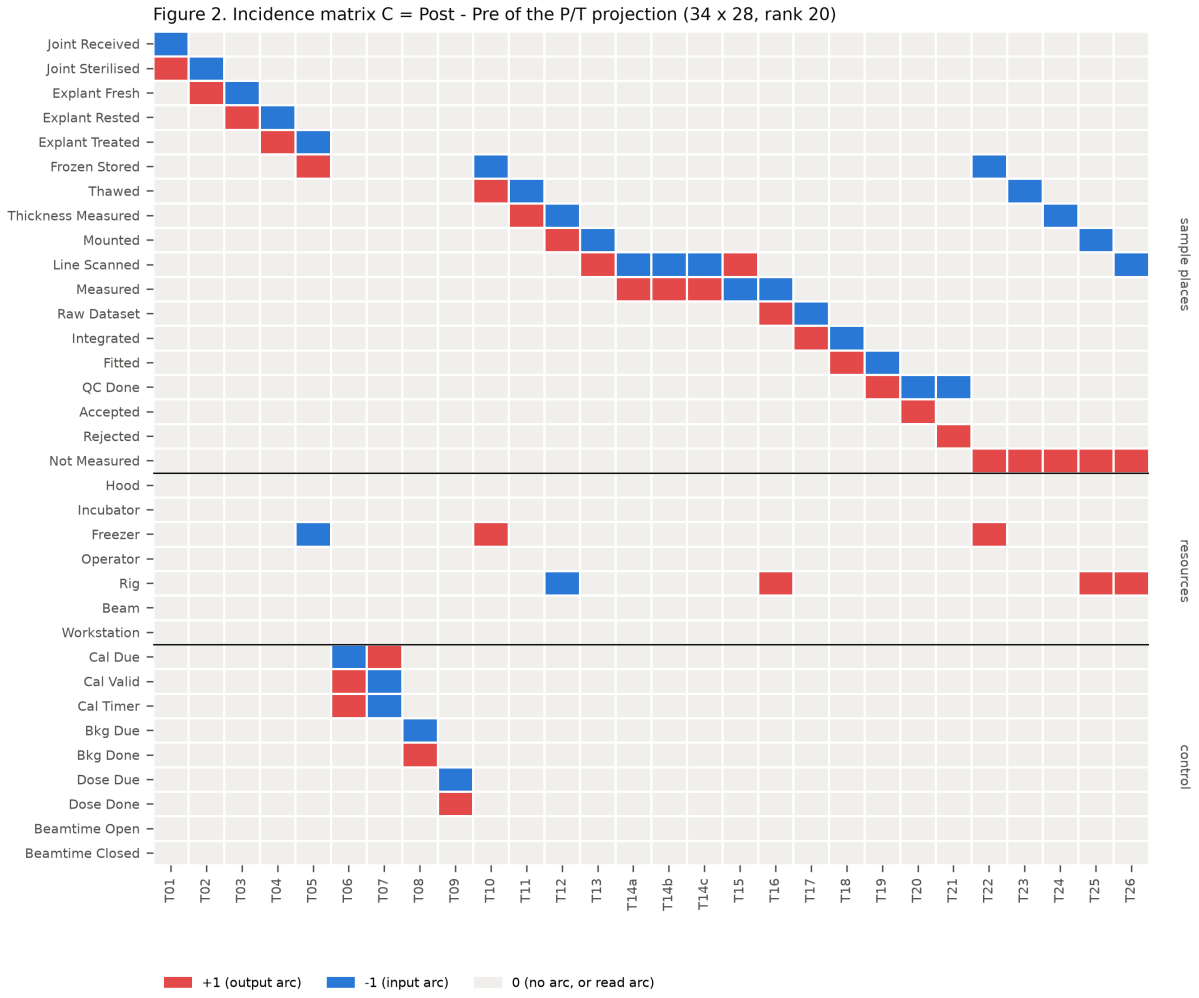


Figure 2. Incidence matrix C = Post - Pre of the Place/Transition projection (34 x 28). Red cells are output arcs, blue cells input arcs; a read arc (consume and return) leaves a zero entry. Horizontal rules separate the sample, resource and control places.

Table 3. Minimal P-semiflows (P1-P14) and T-semiflows (T1-T4) of the projection.

Id	Support	Interpretation
P1	Hood	single resource
P2	Incubator	single resource
P3	Operator	single resource
P4	Beam	single resource
P5	Workstation	single resource
P6	Beamtime_Open	control token
P7	Beamtime_Closed	control token
P8	Frozen_Stored + Freezer	freezer slots
P9	Cal_Due + Cal_Valid	control token
P10	Cal_Due + Cal_Timer	control token
P11	Bkg_Due + Bkg_Done	control token
P12	Dose_Due + Dose_Done	control token
P13	Mounted + Line_Scanned + Measured + Rig	rig occupancy
P14	18 sample places from Joint_Received to Accepted / Rejected / Not_Measured	sample conservation
T1	T14a_Static_Mapping + T15_Remeasure_New_Position	remeasurement cycle
T2	T14b_Stress_Relaxation + T15_Remeasure_New_Position	remeasurement cycle
T3	T14c_Cyclic_Loading + T15_Remeasure_New_Position	remeasurement cycle
T4	T06_Calibrate + T07_Expire_Calibration	calibration cycle

2.6 Simulation experiments

Table 4. Simulation experiments (total 41,900 replications).

Experiment	Factors and levels	Configurations	Replications per configuration	Runs
Baseline synchrotron	48 h beamtime, 2 operators, 0.5 s, pipeline limit 4	1	1000	1000
Baseline laboratory	80 working hours, 1 operator, 3 x 3600 s per explant, sealed cell	1	1000	1000
Factorial	beamtime {24, 48, 72} h x operators {1, 2, 3} x exposure {0.1, 0.5, 2.0} s x pipeline limit {2, 4, 8}	81	200	16,200
One-at-a-time	16 parameters at a low and a high level around the baseline	33	300	9,900
Dose-response	exposure {0.1, 0.25, 0.5, 1, 2, 3, 5, 8} s at relative brightness {1, 20}	16	300	4,800
Laboratory sensitivity	campaign {40, 80, 160} h x exposure per position {1800, 3600, 7200} s x dehydration scale {4, 6, 12} h	27	200	5,400
Explant-level	exposure {0.5, 1.5, 3.0} s x pipeline limit {4, 12} x operators {1, 2}; explant records kept	12	100	1,200
Design robustness	explants per cell {6, 7, 8, 9}; second workstation; pipeline limit {1, 2}	8	300	2,400

Within each experiment the same set of random numbers was used for all configurations (common random numbers). Thus, the different configurations can be compared as paired observations. Running one replication of the baseline takes about 0.1s on one processor core. The full campaign ran in parallel with 18 processor cores within less than 10 minutes.

2.7 Statistical analysis

These replication-level measures were summarized as means and corresponding standard deviations, medians and interquartile ranges as well as 95% bootstrap confidence intervals for means (4000 resamples), and as proportions with corresponding 95% Wilson intervals. Mann-Whitney U tests and corresponding Cliff's deltas were calculated to compare the synchrotron and laboratory baselines. Type II ANOVA and partial eta-squared, a measure of variance for sensitivity, were calculated for the factorial experiment including all main effects and all two-way interactions. The results were complemented by corresponding Kruskal-Wallis tests for each factor. The one-at-a-time experiment was analyzed by calculating paired differences to the corresponding baseline (same seeds) and corresponding bootstrap intervals. The Wilcoxon signed-rank test and corresponding rank-biserial correlations were calculated to test for differences. The dose-response data was compared to the analytical

solution of the lognormal threshold model using the root-mean-square error. Waiting times were fit to a lognormal, gamma and Weibull distribution using maximum-likelihood estimation and compared using the Akaike information criterion (AIC) as well as the corresponding Kolmogorov-Smirnov statistic. Design completion probabilities were calculated as the probability that all 9 cells of the design reached a minimum size. These probabilities were translated into corresponding statistical power for a two-sample t-test with a fixed alpha of 0.05 for a range of standardized effect sizes of 0.8, 1.2 and 1.6, corresponding to the range of D-period and pre-strain effects reported for healthy vs. degraded cartilage explants. Explant-level logistic regressions were used to model the probability of rejection for radiation damage as a function of the log of the dose that was prescribed. The probability of rejection for loss of integrity was modeled as a function of time from thaw to end of measurement. The probability of acceptance was modeled as a function of both plus scenario and group. The corresponding odds ratios including 95% intervals are shown. Convergence of the Monte Carlo simulations was assessed by calculating the running mean and corresponding standard error. All analyses were performed in Python 3.14 using NumPy (1.18), SciPy (1.18), pandas (1.0.1) and stats models (0.15). All figures were created using Matplotlib (3.4.3).

2.8 Comparator selection and evaluation framework

For scattering beamtime, no formal executable model of a workflow is found in the bibliography of this protocol nor in Petri-net literature that we are familiar with. The comparators, therefore, are selected to represent the different classes of models that this protocol relies on: (a) narrative step-by-step how-to protocols like those found in the work of Inamdar et al. (2017, 2019, 2021) and Moger et al. (2007) as well as the two internal how-to documents; (b) the simple exposure-noise rule found in the SAXS Guide where, e.g., noise decreases with the square root of counting time and every measurement is essentially two of them (Schnablegger & Singh, 2011); (c) radiation-damage models that express the dose-dependent change in structure and/or mechanics of collagenous tissues (Barth et al., 2010, 2011) as well as frame-comparison metrics for biological SAXS (Hopkins & Thorne, 2016; Jeffries et al., 2015); (d) the fixed set of storage rules for tissue-preservation found in a number of studies (Szarko et al., 2010; Qu et al., 2014; Kelly et al., 2021; Price et al., 1997); (e) data-analysis models found in the source papers, including: fits of fifth meridional order peak profiles with Gaussian-plus-linear-background models; the linear models D ~ depth + condition

+ depth:condition with type III ANOVA; and orientation statistics (Inamdar et al., 2019; Moger et al., 2007); and processing pipelines like pyFAI, DAWN and Fit2D (Ashiotis et al., 2015; Basham et al., 2015; Hammersley, 2016); (f) formal process-modeling precedents such as: workflow nets; Generalized Stochastic Petri Nets; CPN Tools; and the pre-dialysis TCPN modeled in this study. The comparators were evaluated along the five dimensions used to evaluate clinical pathways in the clinical setting: (1) sample or state representation; (2) workflow coverage; (3) temporal behavior; (4) resource representation; and (5) analytical capability. Predictive accuracy was not used as a criterion because models that answer different questions (e.g., dose-models that compute the probability of certain amounts of damage as a function of dose vs. the process-models computed in this study that ask whether or not a given marking in which the design is complete is reachable from the initial marking within the timeframe of a given beamtime) cannot be compared on this criterion.

3. Results

3.1 Baseline synchrotron beamtime

Figure 3 shows one instance of a baseline experiment where two operators are employed to throw explants into a rolling pipeline of maximum 4. The beam time consists of alternating 2.5min line scans and 16-19min loading periods. The experiment also includes a 12hr refresh of the calibration which is measured after approximately 33hr of beamtime with the last explant. Figure 4 provides a view on the average occupation of all resources over the 1000replications of the experiment. It shows that the operators are the limiting resource (average utilization of 76.6% during beamtime, max. 100%) while the beam (average 41.8%) and the rig (average 27.6%) are idle for more than half of their time. Only the workstations are used to a degree that poses no constraint to the experiments (average 46.0%). Table 5 shows the corresponding descriptive statistics for all resources.

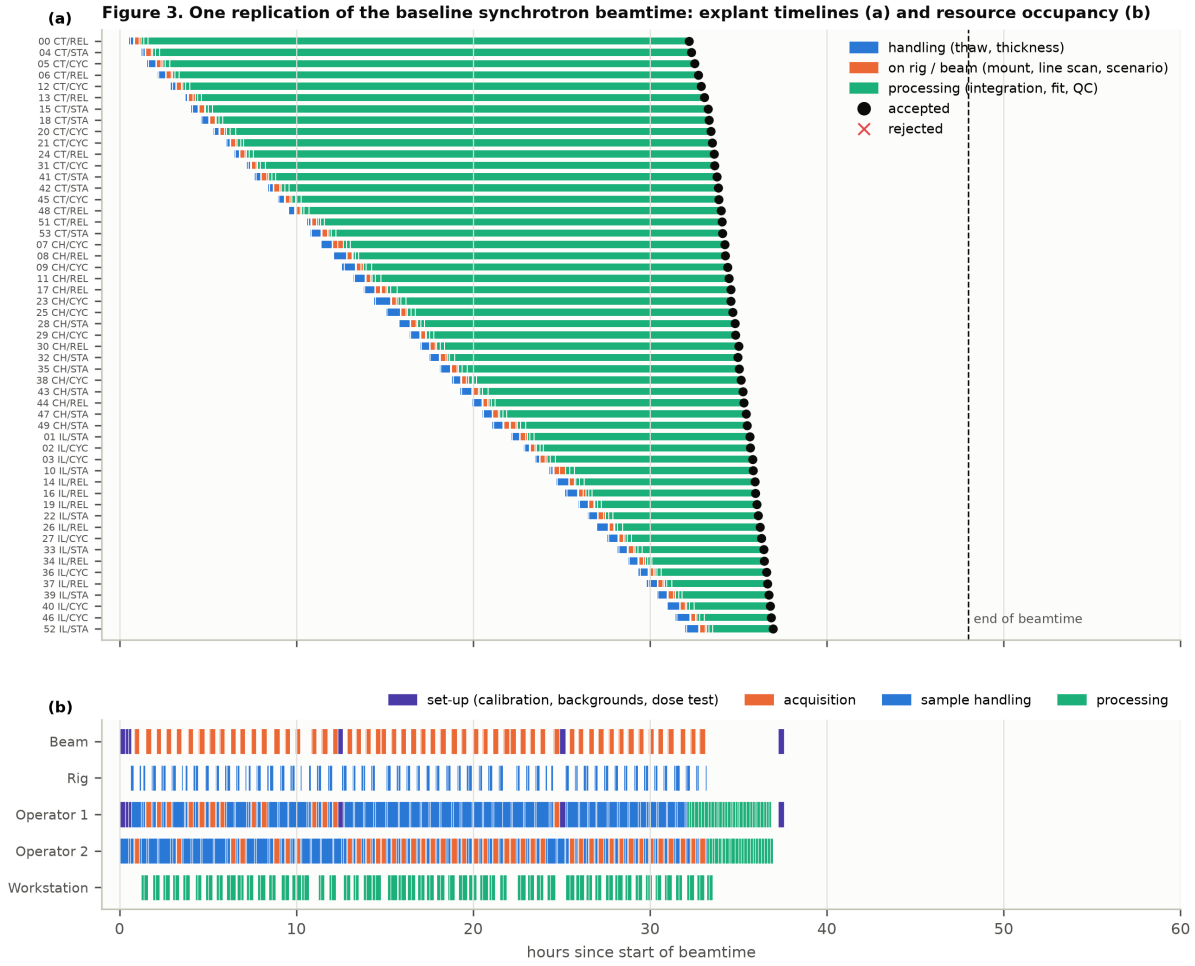


Figure 3. One replication of the baseline synchrotron beamtime (seed 1). (a) Timeline of each of the 54 explants from thaw to outcome, coloured by phase; the long processing segments are datasets waiting for quality control, which the operators defer until acquisition is finished. (b) Occupancy of the beam, the rig, the two operators and the workstation.

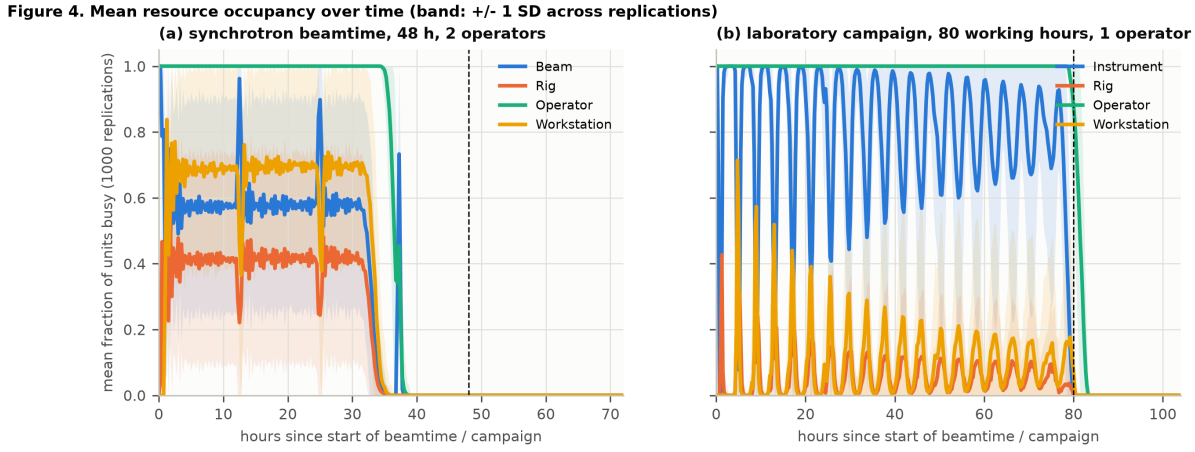


Figure 4. Mean fraction of resource units busy in 15 min bins over 1000 replications (band: one standard deviation). (a) Synchrotron beamtime. (b) Laboratory campaign, where the

instrument occupancy oscillates with the three-hour measurement of each explant and the single operator is saturated.

In the baseline, all 54 explants were measured in every replication (probability of measuring every explant 100.0 %, Wilson interval 99.6 % to 100 %). The mean number of accepted datasets was 50.9 (SD 1.66; 95 % CI 50.8 to 51.0; range 45 to 54), corresponding to a rejection rate of 5.8 % of the measured explants (handling losses 2.0 %, mechanical-synchronization failures 1.9 %, fit failures after a failed remeasurement 1.2 % and losses of integrity 0.7 %). The remeasurement rule was invoked 2.6 times per beamtime on average and recalibration 4 times. The last measurement ended 33.0 h (SD 0.76) after the start of the corresponding allocation block, thus leaving about fifteen hours of the allocation unused.

However, as a design the setup was rarely complete. On average 6.3 of the nine cells had 6 explants left, the smallest cell had 4.7 on average. The probability that all cells of 9 * 6 = 54 explants had 6 explants left was 3.8 % (Wilson interval 2.8 % to 5.2 %), the probability that all cells of 9 * 6 = 54 explants had left at least 4 explants was 97.3 % and for 5 explants left 69.5 %. A loss rate of 6 % on 54 explants thus almost always resulted in the loss of at least one explant from at least one of the nine cells of six explants.

Table 5. Descriptive statistics of the two baselines (1000 replications each; utilizations are fractions of the beamtime or campaign).

Outcome	Synchrotron mean (SD)	95 % CI	median [IQR]	Laboratory mean (SD)	95 % CI	median [IQR]
accepted datasets	50.88 (1.66)	50.78 - 50.99	51.0 [50.0, 52.0]	14.18 (2.08)	14.05 - 14.30	14.0 [13.0, 16.0]
rejected datasets	3.12 (1.66)	3.01 - 3.22	3.0 [2.0, 4.0]	4.28 (1.82)	4.17 - 4.39	4.0 [3.0, 5.0]
explants not measured	0.00 (0.00)	0.00 - 0.00	0.0 [0.0, 0.0]	35.55 (1.01)	35.48 - 35.61	35.0 [35.0, 36.0]
cells with n >= 6 (of 9)	6.28 (1.38)	6.19 - 6.36	6.0 [5.0, 7.0]	0.57 (0.71)	0.53 - 0.61	0.0 [0.0, 1.0]
smallest cell size	4.70 (0.59)	4.66 - 4.74	5.0 [4.0, 5.0]	0.00 (0.00)	0.00 - 0.00	0.0 [0.0, 0.0]
beam / instrument utilization	0.42 (0.01)	0.42 - 0.42	0.4 [0.4, 0.4]	0.79 (0.01)	0.79 - 0.79	0.8 [0.8, 0.8]
rig utilization	0.28 (0.01)	0.28 - 0.28	0.3 [0.3, 0.3]	0.06 (0.00)	0.06 - 0.06	0.1 [0.1, 0.1]
operator utilization	0.77 (0.01)	0.77 - 0.77	0.8 [0.8, 0.8]	1.00 (0.00)	1.00 - 1.00	1.0 [1.0, 1.0]
workstation utilization	0.46 (0.01)	0.46 - 0.46	0.5 [0.5, 0.5]	0.09 (0.01)	0.09 - 0.09	0.1 [0.1, 0.1]
thaw-to-mount wait (min)	75.13 (15.86)	74.12 - 76.12	74.4 [61.7, 87.4]	35.60 (1.54)	35.50 - 35.69	35.5 [34.5, 36.7]
thaw-to-accepted cycle (min)	1125.67 (40.52)	1123.09 - 1128.08	1130.8 [1109.3, 1151.2]	2571.05 (193.27)	2558.74 - 2582.84	2568.8 [2446.1, 2692.6]
time of last measurement (h)	33.02 (0.76)	32.97 - 33.06	33.0 [32.5, 33.5]	78.32 (1.01)	78.26 - 78.38	78.4 [77.8, 79.1]
recalibrations	4.00 (0.00)	4.00 - 4.00	4.0 [4.0, 4.0]	4.00 (0.00)	4.00 - 4.00	4.0 [4.0, 4.0]
remeasurements	2.59 (1.62)	2.49 - 2.69	2.0 [1.0, 4.0]	0.88 (0.88)	0.83 - 0.94	1.0 [0.0, 1.0]

3.2 Baseline laboratory campaign

On the laboratory instrument this design acts very differently (Figure 5). For one operator, three positions of 3600 s per explant and a sealed cell, 14.2 (SD 2.08; 95 % CI 14.1 to 14.3; range 7 to 19) datasets were accepted per 80 working hours. 4.3 datasets were rejected

per 80 hours. 35.5 (66 %) of the explants in the design were never measured. Failure to the experiment was primarily due to dehydration in the sealed cell with 19.1 % of the measured explants failing in this way compared to 2.0 % for handling failure and 1.7 % for synchronization failure. On the instrument the design was busy 79 % of the time whilst the operator was fully utilized 100 % of the time. No replication of the experiment completed a full design cell of four explants. The difference in accepted datasets between the two baselines was 36.7 (95 % CI 36.5 to 36.9; Mann-Whitney test $p < 0.0001$; Cliff's delta 1.00, see above for explanation) gain.

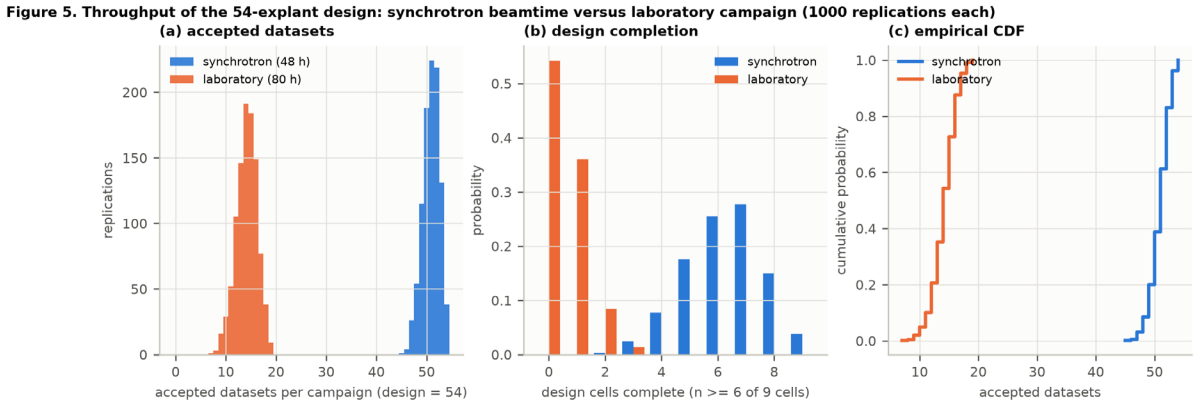


Figure 5. Throughput of the 54-explant design. (a) Distribution of accepted datasets per campaign. (b) Number of design cells that reach six accepted explants. (c) Empirical cumulative distributions.

3.3 Factorial experiment

The mean number of accepted datasets of all 81 configurations ranged from 16.0 (24 h * 1 op * 2 s) to 51.3 (48 h * 3 op * 0.1 s * 2). A least-squares model including all main effects and all two-way interactions explained 96.6 % of the variance between the configurations (cf. Table 6). The most influential parameter was the time allocated for beamtime, followed by the number of operators and their interaction: A single operator needs 72 h to process as many datasets as two operators do within 48 h. A third operator does not add any value, since the pipeline limit and not the number of workers determines the handling rate of the pipeline. The fraction of lost radiation was used to model the effect of exposure time. It turned out to be most influential at 2.0 s (38.1 against 42.0 datasets on average). The integrity losses due to a pipeline limit of eight were modelled by the parameter pipeline limit. The effect turned out to be low with 0.19, but significant ($p = 0.0003$). The respective marginal means are 39.4 and 41.4. Kruskal-Wallis tests confirmed all main effects to be highly significant ($p < 0.0001$).

Table 6. Type II analysis of variance of accepted datasets in the factorial experiment (16,200 runs).

Source	df	Sum of squares	F	p	partial eta-squared
beamtime	2	1325106	151984	$p < 0.0001$	0.949
operators	2	323245	37075	$p < 0.0001$	0.821
exposure	2	60755	6968	$p < 0.0001$	0.463
pipeline limit	2	16958	1945	$p < 0.0001$	0.194
beamtime:operators	4	220770	12661	$p < 0.0001$	0.758
beamtime:exposure	4	7630	438	$p < 0.0001$	0.098
beamtime:pipeline limit	4	1472	84	$p < 0.0001$	0.020
operators:exposure	4	3168	182	$p < 0.0001$	0.043
operators:pipeline limit	4	18151	1041	$p < 0.0001$	0.205
exposure:pipeline limit	4	4609	264	$p < 0.0001$	0.061
Residual	16167	70478			

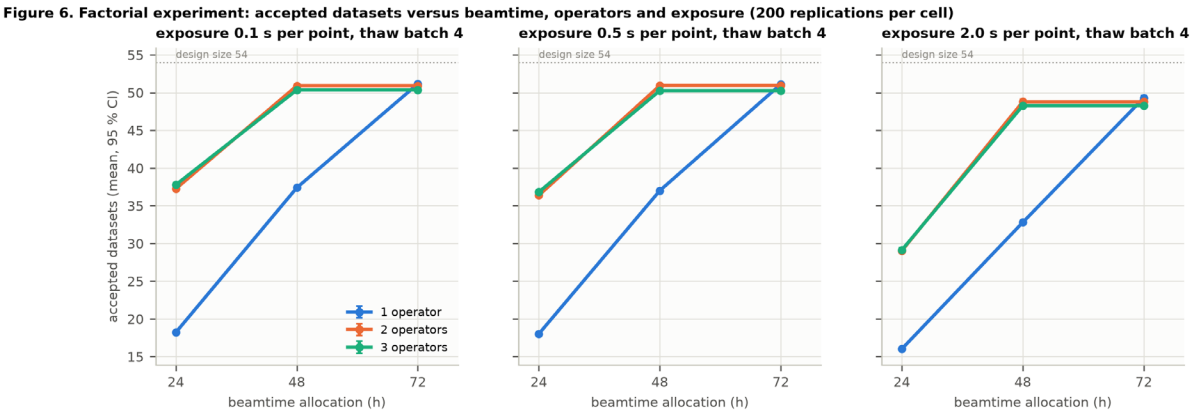


Figure 6. Accepted datasets (mean and 95 % confidence interval) versus beamtime allocation and number of operators, for three exposure times at a pipeline limit of four.

3.4 Outcome profiles

Figure 7 decomposes the fate of the design under eight configurations. Three distinct regimes appear. In the resource-limited regime (24 h with one operator) 65 % of the explants are never measured while the measured ones are almost all accepted. In the dose-limited regime (2.0 s per point) all explants are measured but 1.2 % are lost to radiation damage and 2.8 % to loss of integrity, because the halved-exposure remeasurement lengthens the time explants spend thawed. In the integrity-limited regime (one operator with a pipeline limit of eight) 28 % remain unmeasured and the thawed explants wait longer. The laboratory instrument is time-limited at 3600 s per position (66 % unmeasured) and dehydration-limited at 7200 s (14 % dehydrated, 5 % accepted); only a 160-h campaign with 1800 s per position approaches the synchrotron profile (91 % accepted).

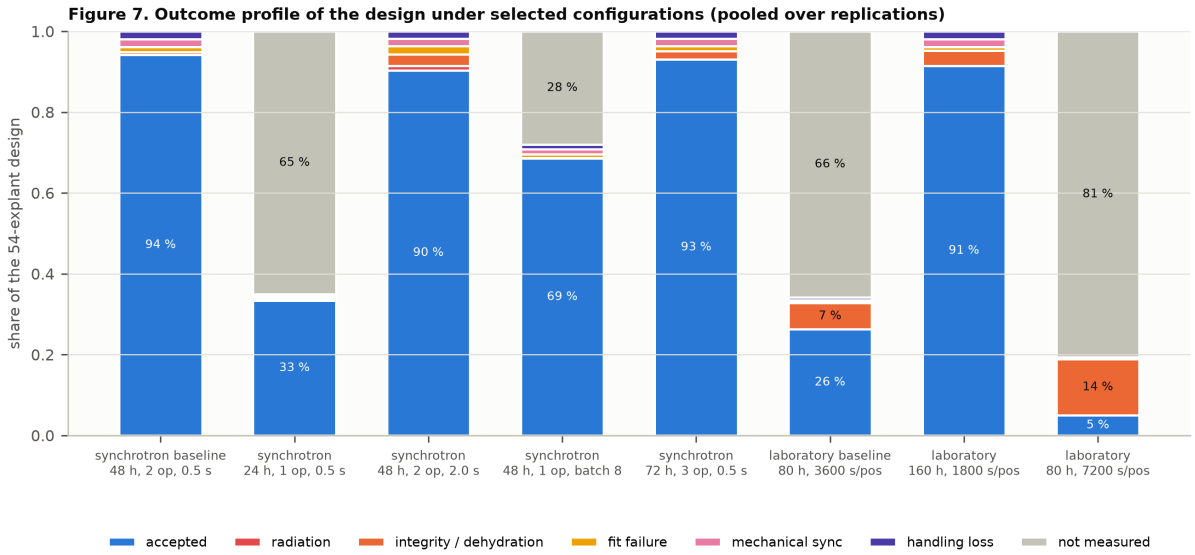


Figure 7. Share of the 54-explant design ending in each outcome, pooled over replications, for selected synchrotron and laboratory configurations.

3.5 One-at-a-time sensitivity

The analysis of sixteen input parameters and their effect on the throughput of the design (number of datasets) is depicted in Figure 8 and in Table 7. As for the design size (number of explants per cell 4 or 9: -16.9 and +23.0 datasets), the beamtime (-14.6 at 24 h) and the number of operators (-14.2 with one operator) are the most dominant parameters in this analysis with a rank-biserial correlation of -1.00 meaning that in all cases the replication was worse than the average. The most important physical parameter in terms of sensitivity to the datasets' loss is the post-thaw integrity scale (Baseline lost -4.7 datasets, 95 % CI -5.1 to -4.4) at a scale of 4 h. In terms of quantitative handling losses of -2.8 (8 %), parasitic scattering of -2.2 (15 %) and exposure of -2.0 (2.0 s) the dataset loss follows in decreasing order. Three operators were found to decrease the throughput by 0.7 ($p < 0.0001$) datasets. As explained before, having more handling capacity than required will keep the pipeline full of thawed explants waiting for the single available rig to become free and integrity losses to rise from 0.39 to 1.04 per beamtime on average. A second rig increased the number of datasets by +0.35, a finer line-scan step of -0.6 (10 micrometers) decreased the number of datasets by 0.6 and a shorter calibration validity of -0.3 (4 h) decreased the number of datasets by 0.3 on average. The variability of the manual steps affected the number of datasets by -0.2 on average. Translation window, no-thaw cut-off and cyclic-loading exposure had no effect on the number of datasets within the investigated ranges.

Table 7. One-at-a-time sensitivity: paired change in accepted datasets relative to the baseline (mean 50.9; 300 paired replications; bootstrap 95 % CI; Wilcoxon signed-rank test).

Parameter	Low value	Change at low [95 % CI]	p	High value	Change at high [95 % CI]	p
beam hours	24	-14.64 [-14.83, -14.42]	p < 0.0001	72	+0.00 [+0.00, +0.00]	p = 1.000
cal validity min	240	-0.25 [-0.49, -0.01]	p = 0.051	1440	+0.06 [-0.15, +0.26]	p = 0.383
cyclic exposure s	0.01	+0.00 [+0.00, +0.00]	p = 1.000	0.1	+0.00 [+0.00, +0.00]	p = 1.000
damage median s	1.5	-0.65 [-0.89, -0.42]	p < 0.0001	10	+0.00 [+0.00, +0.01]	p = 0.317
duration cv	0.05	+0.07 [-0.17, +0.31]	p = 0.425	0.5	-0.16 [-0.40, +0.08]	p = 0.174
exposure s	0.1	+0.07 [-0.15, +0.29]	p = 0.424	2	-2.00 [-2.28, -1.71]	p < 0.0001
handling loss p	0	+0.99 [+0.82, +1.16]	p < 0.0001	0.08	-2.80 [-3.08, -2.52]	p < 0.0001
integrity weibull scale min	240	-4.73 [-5.09, -4.39]	p < 0.0001	1200	+0.31 [+0.24, +0.38]	p < 0.0001
live check fail p	0.01	+0.56 [+0.38, +0.73]	p < 0.0001	0.15	-2.24 [-2.52, -1.97]	p < 0.0001
n operators	1	-14.15 [-14.40, -13.90]	p < 0.0001	3	-0.72 [-1.02, -0.43]	p < 0.0001
n per cell	4	-16.94 [-17.17, -16.71]	p < 0.0001	9	+22.98 [+22.65, +23.29]	p < 0.0001
n rigs	1	+0.00 [+0.00, +0.00]	p = 1.000	2	+0.35 [+0.13, +0.56]	p = 0.0009
step um	10	-0.56 [-0.80, -0.31]	p < 0.0001	50	+0.19 [-0.03, +0.41]	p = 0.049
thaw batch	2	+0.27 [+0.06, +0.48]	p = 0.012	8	-0.05 [-0.16, +0.06]	p = 0.463
thaw cutoff min	45	+0.00 [+0.00, +0.00]	p = 1.000	180	+0.00 [+0.00, +0.00]	p = 1.000
window um	250	+0.00 [-0.02, +0.02]	p = 0.705	1000	+0.00 [+0.00, +0.00]	p = 1.000

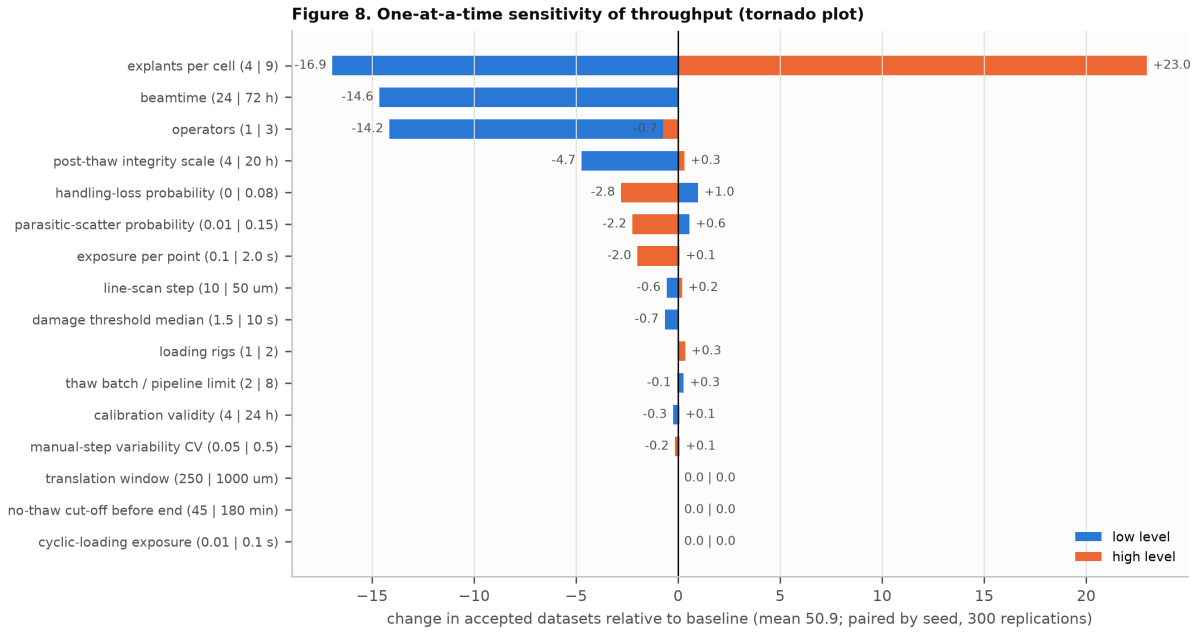


Figure 8. Tornado plot of the one-at-a-time sensitivity of throughput (paired by seed, 300 replications per level).

3.6 Exposure dose-response

The simulated threshold behavior for throughput and radiation damage rejections as a function of exposure per point for two source brightness levels is shown in Figure 9. For

reference brightness, less than 1% rejection of radiation damage explants for all simulated exposures up to 2 s per point (1.0 % on average) and 10% at 3 s per point were found, while the throughput of datasets decreased from 50.9 for 0.5 s to 3.5 for 8 s of exposure. For twenty times brighter source, 1.0% of explants were already rejected at an exposure of 0.1 s per point (on average), 49% at 0.25 s and 94% at 0.5 s. The exposure with less than 5% of radiation damage explants rejected as a function of source brightness is between 2 s at reference brightness and 0.1 s at twenty times brighter source, which in turn brackets the exposure chosen for Diamond I22 (0.5 s) and ESRF ID02 (0.03 s) in the source protocols. The ratio of number of remeasurements, which cost as much beamtime as any other point, to number of points for all simulated conditions is plotted in the right-hand panel of Figure 9. This ratio increased from 2.7 for 0.5 s of exposure per point at reference source brightness to 26.7 for 3 s of exposure per point. The relative differences between the simulated values and the values from lognormal threshold model for one remeasurement of half of the exposure (0.5/2=0.25 s) are plotted in the right-hand panel of Figure 9. The root-mean-square error of these differences is 0.08. Note that several remeasurements, which cost the same amount of beamtime as any other point, were not simulated to end of beamtime for several explants.

Figure 9. Exposure-time dose-response (300 replications per point; threshold median 5 s at reference flux)

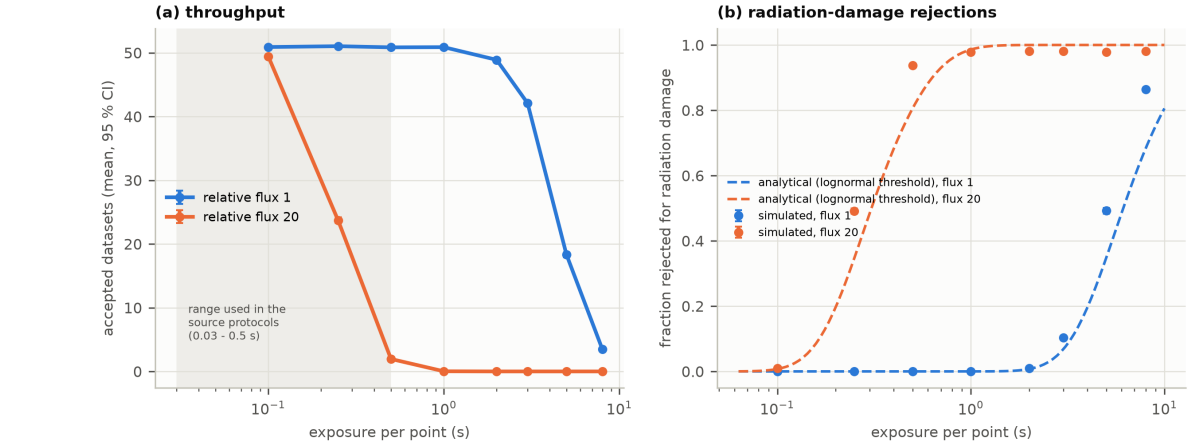


Figure 9. Exposure dose-response at two relative source brightness levels (300 replications per point). (a) Accepted datasets. (b) Fraction of measured explants rejected for radiation damage, with the analytical prediction of the lognormal threshold model (dashed). The shaded band in (a) is the exposure range used in the source protocols.

3.7 Time in system

In the synchrotron baseline scenario (Fig 10) the mean waiting time (from thawing to mounting) is 1.25 h (SD 0.49; median 1.16; interquartile range 0.84 to 1.63 h; maximum 3.21 h) for 52,937 thawed explants. This waiting time can cause integrity losses and does not depend on the loading scenario, see Kruskal-Wallis test p = 0.876. The cycle time from thawing an explant to acceptance of the corresponding dataset has a mean of 18.8 h (SD 7.5) and is almost uniformly distributed between 5 h and 33 h. Thus, a lognormal, gamma or Weibull distribution does not fit this data. Instead, the cycle time can be decomposed into three parts: (1) waiting time in the pipeline of 1.25 h (SD 0.51 h); (2) time on the rig of 0.51 h (SD 0.23 h); and (3) idle time of workstations between the end of the acquisition and acceptance of the corresponding dataset of 17.0 h (SD 7.3 h). Note that (3) is not a workstation backlog since the corresponding workstation is idle more than half of the time. The workstation in Scenario 2 changes the cycle time by +0.03 h (95 % CI -0.00 to +0.07 h; p = 0.304) on average. Thus, (3) corresponds to the quality-control (QC) review, which is carried out by an operator and, thus, has lower priority than acquisition. In order to make thawing explants just-in-time (pipeline limit 1) the cycle time is reduced to 1.9 h (SD 1.4 h). Introducing just-in-time thawing results in integrity losses of 0.09 per beamtime on average, while in the baseline scenario they were 0.42 per beamtime on average. The last measurement is carried out 45.2 h (SD 10.3 h) after the first acquisition (instead of 33.0 h, SD 10.8 h) on average.

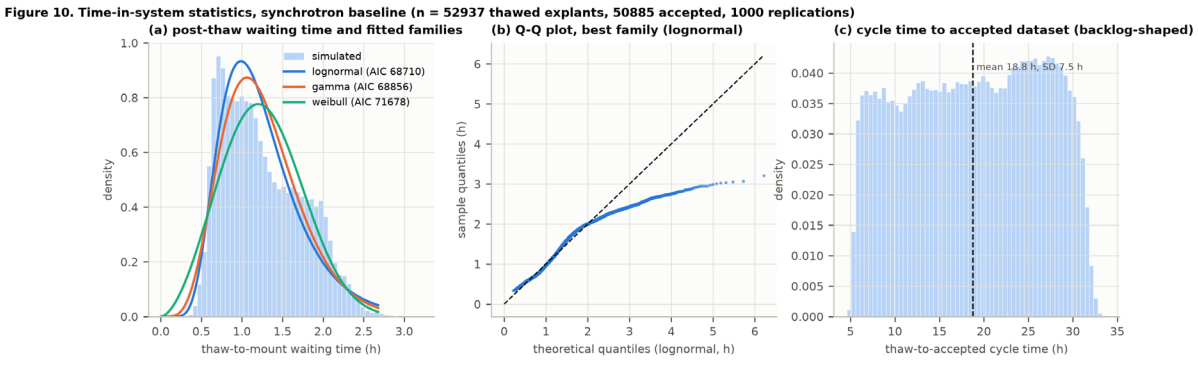


Figure 10. Time-in-system statistics in the synchrotron baseline. (a) Thaw-to-mount waiting time with lognormal, gamma and Weibull maximum-likelihood fits. (b) Quantile-quantile plot against the best family. (c) Thaw-to-accepted cycle time, whose shape is set by the deferral of quality control.

3.8 Design completion, spare explants and statistical power

Fig 11 and Table 8 allow us to translate the number of experiments performed into the quantity of interest for the purposes of the inference, i.e. the number of experimental units that complete the design. There are two operators available to run software. Exposure time is set to 0.5 s and the limit on the number of experiments that can be added to the "pipeline" of experiments awaiting acquisition is set to 4. We found that the probability that all 9 cells had at least 4, 5 or 6 experimental units (for 24h, 48h or 72h designs respectively) was less than 4% for all 3 targets at 24h. For 48h and 72h designs, the probability of all cells having at least 4, 5 or 6 experimental units was 3.5%, 69.5% and 3.5% respectively. Increasing the time to 72h did not change the results for 48h experiments as the "beamtime" was no longer a limiting factor. In order to address this problem, it is therefore sufficient to add spare experimental units to each cell so that, in total, 7 (or 8 or 9) explants are added to each of the 9 cells. Using 7 experimental units per cell (i.e. 63 in total) increases the probability that all cells complete the design to 61% (95%CI = 55% to 66%). The probability increases to 91% (95% CI = 84% to 95%) when 8 experimental units are added per cell (i.e. 72 in total) and to 93% (95% CI = 85% to 97%) when 9 experimental units are added per cell (i.e. 81 in total). At this number of explants per cell the two operators were fully saturated as all experimental units had been added to the design by the time the last experiment had ended after 47.7h. Thus, the most efficient number of experimental units per cell for 48h designs with 2 operators is 8. The power panel shows that the number of cells is also of critical importance when fixing a difference of interest (e.g. the D-period vs. pre-strain difference values reported for healthy and degraded cartilage). Using 6 experimental units per cell (i.e. 54 total) yields a power of 0.47 for a standardized difference of 1.2 (i.e. a difference of 1.2*SD between healthy and degraded cartilage). This increases to 0.39 for a difference of 1.2*SD between healthy and degraded cartilage when 5 experimental units per cell are used (i.e. 45 in total) and to 0.30 for a difference of interest of 1.2*SD between healthy and degraded cartilage when 4 experimental units per cell are used (i.e. 36 in total). A power of 0.8 is reached for a difference of interest of 1.6*SD between healthy and degraded cartilage when 7 experimental units per cell are used (i.e. 63 in total). The power is increased to 0.71 for a difference of interest of 1.2*SD between healthy and degraded cartilage when 6 experimental units per cell are used (i.e. 54 in total). The power increases to 0.89 for a difference of interest of 1.2*SD between healthy and degraded cartilage when 9 experimental units per cell are used (i.e. 81 in total).

Table 8. Design-robustness experiment (48 h, two operators, 300 replications per configuration).

Configuration	Explants	Accepted [95 % CI]	P(all cells n >= 6) [Wilson CI]	Smallest cell	Last measurement (h)	Cycle time (h)	Integrity losses	Unmeasured
baseline	54	50.9 [50.7, 51.1]	0.04 [0.03, 0.07]	4.70	33.0	18.7	0.42	0.0
n_per_cell = 7	63	59.4 [59.2, 59.6]	0.61 [0.55, 0.66]	5.59	38.5	21.6	0.50	0.0
n_per_cell = 8	72	68.0 [67.8, 68.2]	0.91 [0.88, 0.94]	6.41	43.9	24.4	0.57	0.0
n_per_cell = 9	81	74.2 [73.9, 74.4]	0.93 [0.89, 0.95]	6.66	47.7	26.8	0.59	2.4
workstations = 2	54	50.9 [50.7, 51.1]	0.04 [0.03, 0.07]	4.71	33.0	18.7	0.43	0.0
thaw_batch = 1	54	51.1 [50.9, 51.3]	0.07 [0.04, 0.10]	4.75	45.2	1.9	0.09	0.0
thaw_batch = 2	54	51.1 [50.9, 51.3]	0.03 [0.02, 0.06]	4.71	33.4	15.4	0.14	0.0
n_per_cell = 7; workstations = 2	63	59.4 [59.1, 59.6]	0.60 [0.55, 0.66]	5.58	38.5	21.6	0.50	0.0

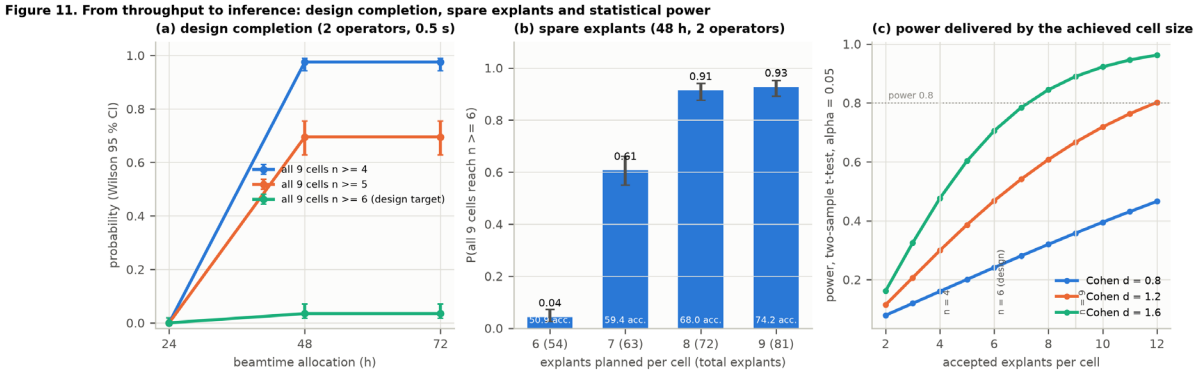


Figure 11. (a) Probability that all nine design cells reach four, five or six accepted explants versus beamtime allocation. (b) Probability of a complete design versus the number of explants prepared per cell. (c) Power of a two-sample t-test versus accepted explants per cell for three standardized effect sizes.

3.9 Monte Carlo convergence

Figure 12 shows the running mean of accepted datasets for both baselines, converging already within the first hundreds of replications. The Monte Carlo standard error of the mean for 1000 replications is 0.053 (ds) for the synchrotron and 0.066 (ds) for the laboratory baseline. These are two orders of magnitude below the effects that have been found. The number of

replications in the sensitivity experiments was chosen to be in the range of 200 to 300 per configuration, resulting in standard errors of below 0.15 datasets.

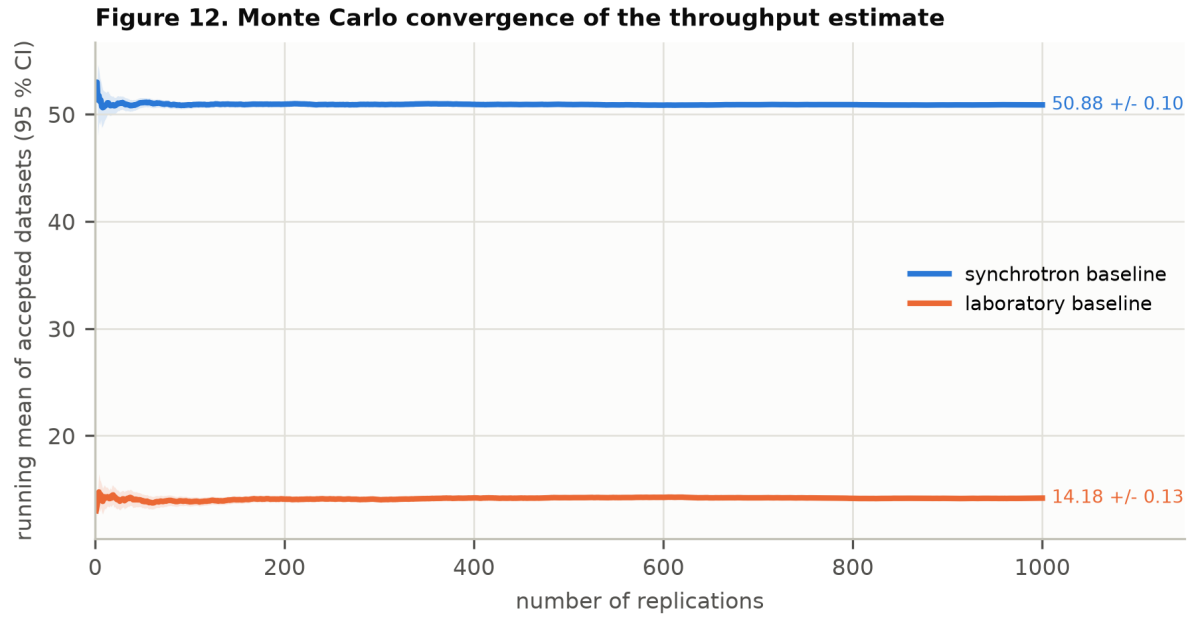


Figure 12. Running mean of accepted datasets with its 95 % confidence interval versus number of replications.

3.10 Laboratory sensitivity

On the laboratory instrument the accepted datasets were almost entirely determined by the three factors exposure per position (partial eta-squared 0.96), campaign length (0.95) and their interaction (0.87), whereas the dehydration time scale entered third (0.71). The model explained 98.3 % of the variance of the observed data (Figure 13). In contrast to the rejection rate of dehydration of 5.4 % of the explants measured at 1800 s per position, the rejection rate of explants increased to 23.2 % at 3600 s and 61.7 % at 7200 s. In contrast to the rejection rate of 4.3 % of the explants at a dehydration time scale of 12 h, the rejection rate of explants increased to 39.1 % at a time scale of 4 h. Only the most favorable cell with a campaign time of 160 h, an exposure per position of 1800 s and a dehydration time scale of 12 h produced the desired number of datasets (51.0). The warning in the second source document must be taken into account, i.e. the ten-hour exposures used for bone are not transferable to hydrated tissue. Measuring three hours per explant at 3600 s per position yielded the highly oscillating instrument occupancy shown in Figure 4b. In summary, it is estimated that there is room for approximately two explants per working day on the instrument.

Table 9. Type II analysis of variance of accepted datasets in the laboratory sensitivity experiment (5,400 runs).

Source	df	Sum of squares	F	p	partial eta-squared
campaign hours	2	400137	53041	p < 0.0001	0.952
exposure per position	2	556676	73792	p < 0.0001	0.965
dehydration scale	2	49157	6516	p < 0.0001	0.708
campaign hours: exposure per position	4	139820	9267	p < 0.0001	0.873
campaign hours: dehydration scale	4	14317	949	p < 0.0001	0.414
exposure per position: dehydration scale	4	9064	601	p < 0.0001	0.309
Residual	5381	20297			

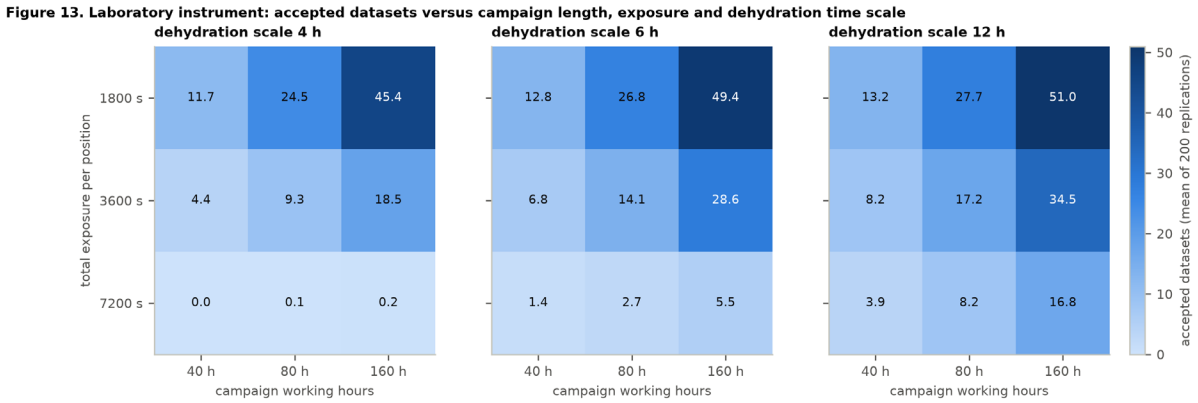


Figure 13. Laboratory instrument: mean accepted datasets versus campaign length and exposure per position, for three dehydration time scales (200 replications per cell).

3.11 Explant-level logistic regression

We analyzed 52,807 explants from 12 different setups, which all were exposed for 0.5, 1.5 or 3 s, had different pipeline limits (4 or 12) and were processed by 1 or 2 people (Fig. 14 and Table 10). As shown in Fig. 14, the probability of rejection due to radiation damage increased dramatically with the prescribed dose. The odds ratio for a one unit change of the natural logarithm of the dose was 3275 (95 % CI: 1336–8024; pseudo R-squared = 0.34) and the dose for 50 % rejection of the explants was estimated to be 7.5 reference-flux seconds. The probability of rejection due to loss of integrity was found to increase with time from thawing to end of measurement. The odds ratio for an one hour increase of time was 1.80 (95 % CI: 1.78–1.83; pseudo R-squared = 0.45) and the time for 50 % rejection was estimated to be 9.4 h, close to the median of the integrity of the Weibull model (8.9 h). In the joint model of acceptance, only dose (odds ratio 0.36 for log dose unit) and time (odds ratio 0.72 for an hour)

were found to be significant. The loading of the samples had a marginal effect, i.e. static mapping had an odds ratio of 1.87 compared to cyclic loading, and the strongest effect was that of the control group having lower odds of acceptance than the chondroitin's treated group. The latter is an artifact of the way the model was specified to reflect the experimental design and is a feature of the protocol that would not be revealed in a narrative representation of the experiment. The strong effect of treatment group on the odds of acceptance of the explants is a confounder, because, in the model as specified, the untreated explants were frozen first, thawed first in a first-in-first-out fashion and therefore wait the longest time in the large thaw batches of the stressed configurations. Thus, treatment group is confounded with waiting time. This is a design flaw that would not be revealed in a narrative protocol and therefore has to be addressed in the design of future experiments. A simple way to address this would be to randomize or block the thaw order of the explants across groups.

Table 10. Explant-level logistic regressions (n = 52,807 measured explants).

Model	**Term**	**Odds ratio**	**95 % CI**	**p**	**pseudo R-squared**
radiation ~ log (prescribed dose)	log dose	3.27e+03	1.34e+03 - 8.02e+03	p < 0.0001	0.341
integrity ~ elapsed time (h)	elapsed time (h)	1.8	1.78 - 1.83	p < 0.0001	0.454
acceptance ~ log dose + elapsed + scenario + group	scenario RELAX	1.74	1.6 - 1.89	p < 0.0001	0.254
acceptance ~ log dose + elapsed + scenario + group	scenario STATIC	1.87	1.72 - 2.03	p < 0.0001	0.254
acceptance ~ log dose + elapsed + scenario + group	group CTRL	0.862	0.8 - 0.929	p = 0.0001	0.254
acceptance ~ log dose + elapsed + scenario + group	group IL1B	0.929	0.856 - 1.01	p = 0.074	0.254
acceptance ~ log dose + elapsed + scenario + group	log dose	0.357	0.336 - 0.379	p < 0.0001	0.254
acceptance ~ log dose + elapsed + scenario + group	elapsed time (h)	0.717	0.708 - 0.726	p < 0.0001	0.254

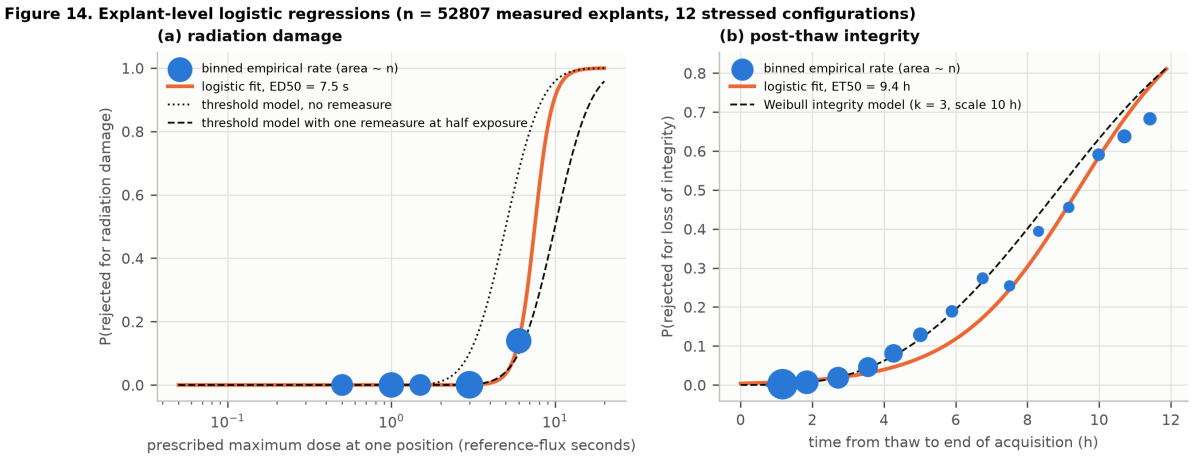


Figure 14. Explant-level logistic regressions. (a) Probability of rejection for radiation damage versus prescribed dose, with the threshold model without and with one halved-exposure remeasurement. (b) Probability of rejection for loss of integrity versus time from thaw to the end of acquisition, with the Weibull integrity model. Marker area is proportional to the number of explants.

4. Comparative Analysis

The TCPN model is compared with the six classes of existing models of Section 2.8, Table 11, with respect to the five dimensions of interest. The existing narrative protocols (Inamdar et al., 2017, 2019, 2021; Moger et al., 2007) of the entire workflow are given as nominal values for all steps of the protocol. The only information about the sample given in the protocols is implicit; time is modeled as a sequence; resources are not modeled at all. Thus, reading the protocols is the only kind of analysis that can be performed with the existing models. The SAXS Guide's exposure–noise rule (Schnablegger & Singh, 2011) and the existing radiation–damage models (Barth et al., 2010, 2011; Hopkins & Thorne, 2016; Jeffries et al., 2015) are quantitative, but local, i.e., an exposure is related to an outcome at a specific position (and explants, and hours, etc. for the remaining positions of the beamline). The preservation studies of the existing models of the source paper (Szarko et al., 2010; Qu et al., 2014; Kelly et al., 2021; Price et al., 1997) establish which storage and handling conditions are admissible, i.e., they define guards for the corresponding transitions. However, the models do not establish any bounds on the waiting time of admissible explants. The data-analysis models of the source papers (Inamdar et al., 2017, 2019, 2021; Moger et al., 2007) of the entire workflow are given as nominal values for all steps of the protocol. The existing data-analysis models of the source papers (Inamdar et al., 2017, 2019, 2021; Moger et al., 2007) of the entire workflow are given

as nominal values for all steps of the protocol. The existing data-analysis models of the source papers (Inamdar et al., 2017, 2019, 2021; Moger et al., 2007) of the entire workflow are given as nominal values for all steps of the protocol. The existing data-analysis models of the source papers (Inamdar et al., 2017, 2019, 2021; Moger et al., 2007) of the entire workflow are given as nominal values for all steps of the protocol. The existing data-analysis models of the source papers (Inamdar et al., 2017, 2019, 2021; Moger et al., 2007) of the entire workflow are given as nominal values for all steps of the protocol.

Note that the TCPN studied in this paper is complementary to the preceding paper protocols: (i) The dose model is used as guard for the live check; (ii) The preservation studies form the integrity sub-model and the thaw transition is enabled if an explant of the corresponding design is still admissible (e.g. stores properly); (iii) The SAXS Guide exposure-noise rule is used to justify the value of the exposure parameters of a sample; (iv) The data-analysis models of the source papers form the consumers of the outcome places of the TCPN. The quantities studied in the TCPN that are not studied in the preceding paper protocols are: (i) the set of states that the beamline is capable of reaching for a given sequence of input transitions; (ii) the probability that a design will complete (i.e. all required measurements will have been taken for all explants of the design); (iii) the binding resource for a transition; (iv) the waiting-time distribution for an explant, i.e. the distribution of the time until it can be processed by the next transition, used as input to study the integrity risk; (v) a failure-mode profile for each configuration. The structural verification of the TCPN adds several important guarantees that cannot be obtained from any simulation: (i) The rig invariant: Two explants cannot be mounted at the same time; (ii) The calibration invariant: The beam is not used with an expired and a valid (for the current time) calibration simultaneously; (iii) The sample invariant: An explant is not lost nor duplicated by the net itself. The TCPN is most like our previous work on a pre-dialysis workflow net (Christoforidis et al., 2026), where patient (explants in the present work), reusable resources, and scenario-parameter delays were modeled as three different types of tokens. Furthermore, the TCPN studied in this work adds three major sub-models to the pre-dialysis model: (i) The dose sub-model; (ii) The integrity sub-model; (iii) A remeasurement loop is added between the slice and dissolve transitions. The model also includes a beamtime window and studies the behavior of the beamline statistically, using Monte Carlo simulations of the generalized stochastic Petri net, as done by (Marsan et al., 1995), and using the timed-token semantics of CPN Tools (Jensen et al., 2007), as done by (van der Aalst, 1998).

Table 11. Comparison of the TCPN with the models in the bibliography of the protocol along five dimensions.

Model class	**Sample / state representation**	**Workflow coverage**	**Temporal behaviour**	**Resource representation**	**Analytical capability**
Narrative protocols (Inamdar 2017, 2019, 2021; Moger 2007; internal documents)	implicit (text, tables)	complete, prescriptive	nominal durations, sequence only	none	reading; manual planning
Exposure-noise rule (SAXS Guide, Schnablegger & Singh 2011)	none	one acquisition	counting time vs noise	none	choice of exposure time
Radiation-damage models (Barth 2010, 2011; Hopkins & Thorne 2016; Jeffries 2015)	dose per position	one acquisition	dose rate, frame series	none	damage probability, frame-comparison metrics
Preservation studies (Szarko 2010; Qu 2014; Kelly 2021; Price 1997)	storage state	preparation only	freeze-thaw cycles, storage duration	none	admissible conditions (guards)
Data-analysis models (Gaussian fits; D ~ depth + condition, type III ANOVA; pyFAI, DAWN, Fit2D)	dataset	processing only	none	none (workstation implicit)	parameter estimation, hypothesis tests
Formal precedents (workflow nets; GSPN; CPN Tools; pre-dialysis TCPN)	tokens with colour	generic / clinical pathway	timed tokens, stochastic delays	resource tokens	invariants, reachability, simulation
Present TCPN	coloured explant token (group, scenario, dose, threshold, integrity time, flags)	joint receipt to accepted dataset, three scenarios, remeasurement, end of beamtime	timed tokens; minutes to days; beamtime window; calibration validity	hood, incubator, freezer, operators, rig, beam, workstation	P/T-invariants, boundedness; Monte Carlo throughput, completion probability, power, sensitivity, dose-response, logistic risk models

5. Discussion

One key result that the model provides over and above the protocol is that of two different goals the narrative protocol does not distinguish between them: measuring all explants and completing the design. So, under our ‘base case’ assumptions the beamtime on the synchrotron to measure all explants of a given sample has a loss rate of six percent or so, a completely successful experiment. Yet in less than four percent of cases the resulting design is complete – 9 cells of 6 explants each. To achieve a probability of complete design of over ninety percent the model calculates that with 48-hour beamtime and two people to make the punches, eight explants per cell would suffice for a total of twelve extra punches, but no extra beamtime. In contrast, 24-hour beamtime cannot be used to complete the design with any number of operators, and interestingly the presence of a third operator to act as back-up to the planner actually reduces the percentage complete design slightly, because he fills the handling pipeline and extends the post-thaw waiting time to the operating limit for the personnel on duty.

Our analysis further defines two key areas of the beamline’s operation: the binding resources of the facility (i.e. those that cannot be varied within the current set of operating points) and the dominant failure mode for each set of operating conditions. As for radiation damage, in the case of the exposures specified in the source protocols’ ‘exposure’ field, it simply is not a failure mode at all: the dose test and remeasurement rule specified in the protocols are a safeguard that has no value whatsoever until the ‘brightness’ or ‘exposure’ of the source is increased, and the model generates the two published operating points as safe limits for the relevant increases. By contrast, the waiting time after thawing an explant is a failure mode that the protocol does not explicitly control: it is set by the operator’s policy on how many samples to thaw ahead of time, it is a lognormally distributed variable whose tail is truncated by the above policy, and it is the major cause of loss whenever the pipeline fills. We also found a confound between treatment group and waiting time in the first-in-first-out (FIFO) policy of thawing samples frozen in group order; this is an easily fixed problem, and we have recommended that samples be thawed in random or blocked order.

Within the laboratory, the ten-hour exposures originally used for bone samples are not long enough for measurements on hydrated tissue samples. This was already stated in the second source document. Here too, the amount of time available for measurement with a given number of explants is limited by the time spent positioning the samples in the beam. For 3600 s per position and 3 positions per explant, this amounts to 2 explants per working day.

Dehydration of the samples in the sealed cells occurs to the extent of about 20%. Considering the delay caused by the handling pipeline, none of the cells of the intended design can be completed with the current settings. Shortening the exposure time to 1800 s and increasing the campaign to twice the size of the current one leads to a recovery of the synchrotron radiation profile at the cost of lower signal-to-noise, which can be converted to a penalty using the SAXS Guide rule. As such, the best instrument for the pilot measurements (fresh vs. frozen-thawed, healthy vs. trypsin-treated, steady state before and after loading) is the laboratory instrument.

Formal transparency: The major assumptions, transition conditions, resources and delays are all laid bare for dispute. For the hybrid architecture to be implemented according to the structure of Section 4, an empirical dose model, to predict dose at the beamline, could be developed to substitute for the long-distributor threshold (Fratzl et al., 1998). In similar manner to Hopkins and Thorne (2016) for frame comparison, an integrity model could also be created to best predict D-period and proteoglycan content with time after thaw of explants for the Weibull to be replaced by empirical integrity model. Durations of individual actions could be estimated from the beamline's log of past actions and the resulting net would predict, prior to each beamtime, the probability of a complete design, the number of additional explants to have punched for ‘spare’ samples, the best policy for their thawing and the optimal exposure for best signal-to-dose ratio, and predicted sizes of individual cells to input into power calculations for the planned statistical analysis.

5.1 Limitations

Several key limitations of this paper have to be noted by the reader: (1) The TCPN is a conceptual model and thus it has not been fitted to logs from real beamtime. Even if the structural correctness of the model is granted, this does not necessarily imply that its throughput predictions are accurate for realistic input. The numbers in the tables are properties of the scenario and have to be checked for realism for a specific application; (2) All timing, damage threshold, integrity time, probabilities for handling loss, parasitic scattering, and synchronization failures as well as the laboratory working-hour calendar have been chosen as illustrative values and have been anchored to specific statements in the documents (0.1 to 5 s linear response time at I22, 0.03 s at ID02, 1 min test frames plus summed short frames in the lab, 3600 s per position for powders) whereas the empirical application has to use validated distributions for these variables, again performing a sensitivity/uncertainty analysis; (3) The color of an explant only shows a very small part of the complete state, namely not the zone that

is currently measured, the thickness, the real D-period (with its uncertainty) as well as the number of depth bins that where actually usable (i.e. not on the plate edges) for the measurement; the measurement itself can even be scientifically correct but statistically too weak; (4) All resources have been strongly simplified, i.e. all operators are interchangeable, they never get tired, the beam never fails and never is refilled, the calibration drift has a fixed validity window, and a workstation processes all datasets from all operators without any human interaction; (5) The dose sub-model only counts the exposures on a position and does not take into account the dose rate as well as the beam-size dependent damage, the cumulative dose on neighboring positions, as well as the slow damage reported in the frame-comparison literature. WAXS measurements have not been modelled as there are no source studies on cartilage using this type of measurement; (6) The ordinary 34x28 projection does not preserve information: a transition that changes the color but not the place of a token (i.e. dose accumulation, exposure halving, flags, single-thaw counter) as well as a joint token being transformed into several explant tokens of the same position cannot be verified to have the required properties using color-refined state-space analysis; this has been verified by simulation only for the attributes used in this paper; (7) All operator policies (thawing: FIFO, acquisition: first quality control measurement for a sample acquired, pipeline: fixed size) have been chosen by the author for reasons of simplicity and have to be replaced by more realistic ones for a realistic verification, as they introduce a confound that has been reported in Section 3.11 already; (8) The comparison to other models in the bibliography is methodological in nature and thus not a performance comparison in terms of accuracy on a given data set, as a dose model and a process model cannot be ranked on the basis of a single accuracy metric.

6. Conclusion

We present a timed Coloured Petri Net (TCPN) formal representation of the SAXS/WAXS measurement protocol for hydrated articular cartilage samples. The Net has 34 places and 28 transitions which represent all steps (preparation, measurement, processing, quality-check) of the protocol as encoded from literature sources. The place invariants of the Net encode the following constraints of the protocol: there are as many explants leaving as were prepared, there are as many loading rig bookings as there are measurements, and there are as many calibrated instruments as there are configured. The execution of the Net in 41,900 Monte Carlo runs gives quantitative measures for the number of samples, failures, resources, waiting times, design completion and statistical power for both a synchrotron beamtime and a lab campaign. The TCPN representation of the protocol is more detailed than the protocols given

in literature as well as the dose and preservation models and peak-fitting statistics given in the bibliography as single steps or even single constraints to the workflow. But while the narrative protocols, dose and preservation models and peak-fitting statistics given in literature allow to check single steps or even single constraints for the workflow, the TCPN gives a complete representation of the whole workflow under time and resource constraints. Hence the TCPN is the only representation among them which allows to check in advance of a beamtime whether a design is implementable and how many spare explants, operators and hours of time are required for the given design. The most promising use of the TCPN is as a formally verified process model where empirical dose, integrity and duration models are used as parameters for the guards and delays of the transitions.

Data and code availability

The Python implementation of the timed CPN engine (tcpn.py), the protocol model (saxs_cpn.py), the structural analysis (structural.py), the experiment driver (experiments.py), the statistical analysis (analysis.py), the figure scripts, the replication-level and explant-level result files and all figures are provided with this manuscript in the model, results and figures folders.

References

ASHIOTIS, G., DESCHILDRE, A., NAWAZ, Z., WRIGHT, J. P., KARKOULIS, D., PICCA, F. E., & KIEFFER, J. (2015). The fast azimuthal integration Python library: pyFAI. Journal of Applied Crystallography, 48(2), 510-519. https://doi.org/10.1107/S1600576715004306

BARTH, H. D., LAUNEY, M. E., MACDOWELL, A. A., AGER, J. W., & RITCHIE, R. O. (2010). On the effect of X-ray irradiation on the deformation and fracture behavior of human cortical bone. Bone, 46(6), 1475-1485. https://doi.org/10.1016/j.bone.2010.02.025

BARTH, H. D., ZIMMERMANN, E. A., SCHAIBLE, E., TANG, S. Y., ALLISTON, T., & RITCHIE, R. O. (2011). Characterization of the effects of x-ray irradiation on the hierarchical structure and mechanical properties of human cortical bone. Biomaterials, 32(34), 8892-8904. https://doi.org/10.1016/j.biomaterials.2011.08.013

BASHAM, M., FILIK, J., WHARMBY, M. T., CHANG, P. C. Y., EL KASSABY, B., GERRING, M., AISHIMA, J., LEVIK, K., PULFORD, B. C. A., SIKHARULIDZE, I., SNEDDON, D., WEBBER, M., DHESI, S. S., MACCHEROZZI, F., SVENSSON, O., BROCKHAUSER, S., NARAY, G., & ASHTON, A. W. (2015). Data Analysis WorkbeNch (DAWN). Journal of Synchrotron Radiation, 22(3), 853-858. https://doi.org/10.1107/S1600577515002283

CHRISTOFORIDIS, S., THOMOPOULOS, A., TITOPOULOS, E., KROMITOGLOU, E., CHATZIPRODROMOU, M. I., ILIEVA, B., & STANCHEV, G. (2026). A timed Color Petri Net model for the pre-dialysis clinical pathway in chronic kidney disease: Comparison with contemporary predictive modelling approaches. Manuscript in preparation.

COLOM, J. M., & SILVA, M. (1991). Convex geometry and semiflows in P/T nets: A comparative study of algorithms for computation of minimal P-semiflows. In G. Rozenberg (Ed.), Advances in Petri Nets 1990 (Lecture Notes in Computer Science, Vol. 483, pp. 79-112). Springer. https://doi.org/10.1007/3-540-53863-1_22

FRATZL, P., MISOF, K., ZIZAK, I., RAPP, G., AMENITSCH, H., & BERNSTORFF, S. (1998). Fibrillar structure and mechanical properties of collagen. Journal of Structural Biology, 122(1-2), 119-122. https://doi.org/10.1006/jsbi.1998.3966

GIANNINI, C., SILIQI, D., LADISA, M., ALTAMURA, D., DIAZ, A., BERAUDI, A., SIBILLANO, T., DE CARO, L., STEA, S., BARUFFALDI, F., & BUNK, O. (2014). Scanning SAXS-WAXS microscopy on osteoarthritis-affected bone: An age-related study. Journal of Applied Crystallography, 47(1), 110-117. https://doi.org/10.1107/S1600576713030215

HAMMERSLEY, A. P. (2016). FIT2D: A multi-purpose data reduction, analysis and visualization program. Journal of Applied Crystallography, 49(2), 646-652. https://doi.org/10.1107/S1600576716000455

HEPHAESTUS LABORATORY, DEMOCRITUS UNIVERSITY OF THRACE. (2026). SAXS/WAXS measurement protocol for biological samples: Cartilage, bone, hair, nails, skin and faeces (internal protocol draft for discussion with the Hephaestus Laboratory, Kavala).

HOPKINS, J. B., & THORNE, R. E. (2016). Quantifying radiation damage in biomolecular small-angle X-ray scattering. Journal of Applied Crystallography, 49(3), 880-890. https://doi.org/10.1107/S1600576716005136

INAMDAR, S. R., BARBIERI, E., TERRILL, N. J., KNIGHT, M. M., & GUPTA, H. S. (2019). Proteoglycan degradation mimics static compression by altering the natural gradients in fibrillar organisation in cartilage. Acta Biomaterialia, 97, 437-450. https://doi.org/10.1016/j.actbio.2019.07.055

INAMDAR, S. R., KNIGHT, D. P., TERRILL, N. J., KARUNARATNE, A., CACHO-NERIN, F., KNIGHT, M. M., & GUPTA, H. S. (2017). The secret life of collagen: Temporal changes in nanoscale fibrillar pre-strain and molecular organization during physiological loading of cartilage. ACS Nano, 11(10), 9728-9737. https://doi.org/10.1021/acsnano.7b00563

INAMDAR, S. R., PREVOST, S., TERRILL, N. J., KNIGHT, M. M., & GUPTA, H. S. (2021). Reversible changes in the 3D collagen fibril architecture during cyclic loading of healthy and degraded cartilage. Acta Biomaterialia, 136, 314-326. https://doi.org/10.1016/j.actbio.2021.09.037

JEFFRIES, C. M., GRAEWERT, M. A., SVERGUN, D. I., & BLANCHET, C. E. (2015). Limiting radiation damage for high-brilliance biological solution scattering: Practical experience at the EMBL P12 beamline PETRAIII. Journal of Synchrotron Radiation, 22(2), 273-279. https://doi.org/10.1107/S1600577515000375

JENSEN, K., & KRISTENSEN, L. M. (2009). Coloured Petri nets: Modelling and validation of concurrent systems. Springer. https://doi.org/10.1007/b95112

JENSEN, K., KRISTENSEN, L. M., & WELLS, L. (2007). Coloured Petri Nets and CPN Tools for modelling and validation of concurrent systems. International Journal on Software Tools for Technology Transfer, 9(3-4), 213-254. https://doi.org/10.1007/s10009-007-0038-x

KELLY, S. J., DUPLESSIS, L., SOLEY, J., NOBLE, F., WELLS, H. C., & KELLY, P. J. (2021). Pilot study on the effects of preservatives on corneal collagen parameters measured by small angle X-ray scattering analysis. BMC Research Notes, 14, 78. https://doi.org/10.1186/s13104-021-05494-y

LAW, A. M. (2015). Simulation modeling and analysis (5th ed.). McGraw-Hill Education.

Marsan, M. A., Balbo, G., Conte, G., Donatelli, S., & Franceschinis, G. (1995). Modelling with generalized stochastic Petri nets. Wiley.

MARTINEZ, J., & SILVA, M. (1982). A simple and fast algorithm to obtain all invariants of a generalised Petri net. In C. Girault & W. Reisig (Eds.), Application and theory of Petri nets

(Informatik-Fachberichte, Vol. 52, pp. 301-310). Springer. https://doi.org/10.1007/978-3-642-68353-4_47

MOGER, C. J., BARRETT, R., BLEUET, P., BRADLEY, D. A., ELLIS, R. E., GREEN, E. M., KNAPP, K. M., MUTHUVELU, P., & WINLOVE, C. P. (2007). Regional variations of collagen orientation in normal and diseased articular cartilage and subchondral bone determined using small angle X-ray scattering (SAXS). Osteoarthritis and Cartilage, 15(6), 682-687. https://doi.org/10.1016/j.joca.2006.12.006

MUEHLEMAN, C., MAJUMDAR, S., ISSEVER, A. S., ARFELLI, F., MENK, R.-H., RIGON, L., HEITNER, G., REIME, B., METGE, J., WAGNER, A., KUETTNER, K. E., & MOLLENHAUER, J. (2004). X-ray detection of structural orientation in human articular cartilage. Osteoarthritis and Cartilage, 12(2), 97-105. https://doi.org/10.1016/j.joca.2003.10.001

MURATA, T. (1989). Petri nets: Properties, analysis and applications. Proceedings of the IEEE, 77(4), 541-580. https://doi.org/10.1109/5.24143

PABISCH, S., WAGERMAIER, W., ZANDER, T., LI, C., & FRATZL, P. (2013). Imaging the nanostructure of bone and dentin through small- and wide-angle X-ray scattering. Methods in Enzymology, 532, 391-413. https://doi.org/10.1016/B978-0-12-416617-2.00018-7

PRICE, R. I., LEES, S., & KIRSCHNER, D. A. (1997). X-ray diffraction analysis of tendon collagen at ambient and cryogenic temperatures: Role of hydration. International Journal of Biological Macromolecules, 20(1), 23-33.

QU, C., HIRVINIEMI, M., TIITU, V., JURVELIN, J. S., TOYRAS, J., & LAMMI, M. J. (2014). Effects of freeze-thaw cycle with and without proteolysis inhibitors and cryopreservant on the biochemical and biomechanical properties of articular cartilage. Cartilage, 5(2), 97-106. https://doi.org/10.1177/1947603513515998

RINNERTHALER, S., ROSCHGER, P., JAKOB, H. F., NADER, A., KLAUSHOFER, K., & FRATZL, P. (1999). Scanning small angle X-ray scattering analysis of human bone sections. Calcified Tissue International, 64(5), 422-429. https://doi.org/10.1007/PL00005824

SAXS/WAXS measurement protocol for articular cartilage: Literature review. (2026, October 1). Internal document synthesising nine publications into a measurement protocol (sample preparation, set-up, measurement sequence, analysis and quality control).

SCHNABLEGGER, H., & SINGH, Y. (2011). The SAXS guide: Getting acquainted with the principles (2nd ed.). Anton Paar GmbH.

SZARKO, M., MULDREW, K., & BERTRAM, J. E. A. (2010). Freeze-thaw treatment effects on the dynamic mechanical properties of articular cartilage. BMC Musculoskeletal Disorders, 11, 231. https://doi.org/10.1186/1471-2474-11-231

van der Aalst, W. M. P. (1998). The application of Petri nets to workflow management. Journal of Circuits, Systems and Computers, 8(1), 21-66. https://doi.org/10.1142/S0218126698000043

ZIZAK, I., ROSCHGER, P., PARIS, O., MISOF, B. M., BERZLANOVICH, A., BERNSTORFF, S., AMENITSCH, H., KLAUSHOFER, K., & FRATZL, P. (2003). Characteristics of mineral particles in the human bone/cartilage interface. Journal of Structural Biology, 141(3), 208-217. https://doi.org/10.1016/S1047-8477(02)00635-4

Sofoklis Christoforidis

ORCID iD: 0009-0000-9818-8264

Technical University of Sofia, Bulgaria

Email: sofoklis.christoforidis@gmail.com

Efstathios Titopoulos,

ORCID iD: 0000-0003-4084-1675

Technical University of Sofia, Bulgaria

Email: titopoulos@lot-consult.com

Dr. Georgi Stanchev, Assos. Prof.

Department „Fundamentals and Technical Means of Design”,

Technical University of Sofia,

Bulgaria

E-mail: gstanchev@tu-sofia.bg

Dr. Assoc. Prof. Boryana Petkova Ilieva-Mihailova,

Department „Fundamentals and Technical Means of Design”,

TU-Sofia , Bulgaria

E-mail: bilieva@tu-sofia.bg

Eleni Kromitoglou

ORCID iD: 0009-0000-2789-1112

Democritus University of Thrace, Kavala, Greece

Email:elkromi@mst.duth.gr

Dimosthenis Pappas,

ORCID iD: 0009-0009-1950-7200

Democritus University of Thrace, Kavala, Greece

Email: dpappas@admin.duth.gr